

# Climbing Stairs with Humanoid Robots

Semesterarbeit

an der Fakultät für Maschinenwesen der Technischen Universität München

**Betreut von** Prof. dr.ir. Daniel J. Rixen, M.Sc.  
Arne-Christoph Hildebrandt, M.Sc.  
Lehrstuhl für Angewandte Mechanik

**Eingereicht von** Konstantin Ritt  
Brunnerstraße 37  
80804 München

**Eingereicht am** Garching, den 30. Oktober 2016



# Contents

- 1 Introduction** **2**
  - 1.1 Situation and Motivation . . . . . 2
  - 1.2 Concept . . . . . 2
  
- 2 Overview and Related Work** **4**
  - 2.1 Pattern Generation . . . . . 4
  - 2.2 Variable Center of Mass (CoM) Height . . . . . 6
    - 2.2.1 Motivation . . . . . 6
    - 2.2.2 Modeling Approaches . . . . . 6
    - 2.2.3 Trajectory Design . . . . . 8
  
- 3 Vertical Center of Mass (CoM) Trajectory Generation** **11**
  - 3.1 Current Situation and General Assumptions . . . . . 12
  - 3.2 Step Phase . . . . . 13
  - 3.3 Maximum Hip Height . . . . . 14
  - 3.4 Initial Hip Trajectory . . . . . 15
    - 3.4.1 Requirements . . . . . 15
    - 3.4.2 Cubic Splines . . . . . 16
    - 3.4.3 Constraints and Support Points . . . . . 17
  - 3.5 Optimization . . . . . 19
    - 3.5.1 Extended Time Horizon . . . . . 20
    - 3.5.2 Cost Function . . . . . 21
    - 3.5.3 Underlying Geometric Model . . . . . 23
  
- 4 Evaluation** **25**

4.1	Assumptions and Test Environment . . . . .	25
4.1.1	Input Trajectories . . . . .	25
4.1.2	Solver . . . . .	28
4.1.3	Shortcomings . . . . .	28
4.2	Optimal Amount of Predicted Steps . . . . .	28
4.3	Comparison to Current Approach . . . . .	32
4.3.1	Even Walking . . . . .	33
4.3.2	Upstairs . . . . .	34
4.3.3	Downstairs . . . . .	36
4.4	Discussion . . . . .	39
4.4.1	Input Trajectories . . . . .	39
4.4.2	Flawed Initial Solution . . . . .	40
4.4.3	Performance . . . . .	42
<b>5</b>	<b>Conclusion</b>	<b>43</b>
<b>A</b>	<b>Additional Plots</b>	<b>44</b>
	<b>References</b>	<b>49</b>

## List of Figures

3.1	Overview of newly proposed trajectory generation system and section of pattern generation that gets replaced . . . . .	12
3.2	Step sequences . . . . .	13
3.3	Kinematically feasible maximum height . . . . .	14
3.4	Maximum hip height for swing and stance leg for 3 steps upstairs with $\Delta z = 0.1m$ .	15
3.5	Choice of support points, here upstairs with $\Delta z = 0.15m$ . . . . .	17
3.6	Choice of tuning parameter $p_{tune}$ . . . . .	19
3.7	Initial conditions for upstairs movement with $\Delta z = 0.05m$ for $n = 2$ Steps . . . . .	20
3.8	Differing step command after $t = 3$ leads to change propagation to $z_{hip}$ trajectories before $t = 3$ . . . . .	21
3.9	Angle limit cost function . . . . .	22
3.10	2D geometric model for obtaining joint angles and velocities . . . . .	23
4.1	Input and output for MATLAB model . . . . .	25
4.2	Foot trajectory in x-direction with $\Delta x = 0.5m$ . . . . .	26
4.3	Foot trajectory in z-direction for upstairs with $\Delta z = 0.1$ . . . . .	27
4.4	Foot and hip trajectory in x-direction . . . . .	27
4.5	Performance of converged solution depending on steps considered in preview period for even walking . . . . .	29
4.6	Trajectory generation failure for preview horizon of one step, displaying trajectories for two steps . . . . .	29
4.7	Performance of converged solution depending on steps considered in preview period for upstairs movement ( $\Delta z = 0.1m$ ) . . . . .	30
4.8	Performance of converged solution depending on steps considered in preview period for downstairs movement ( $\Delta z = -0.1m$ ) . . . . .	31
4.9	Convergence rate for even walking with $\Delta x = 0.4m$ . . . . .	31
4.10	Convergence rate for upstairs scenario with $\Delta x = 0.5m$ . . . . .	32

4.11	Convergence rate for downstairs scenario with $\Delta x = 0.5m$ . . . . .	32
4.12	Comparison of height trajectories for step size $\Delta x = 0.4m$ . . . . .	33
4.13	Comparison of height trajectories for step size $\Delta x = 0.6m$ . . . . .	34
4.14	Comparison of knee joint angles of swing leg for step size $\Delta x = 0.6m$ . . . . .	34
4.15	Comparison of height trajectories for upstairs movement with step size $\Delta x = 0.4m$	35
4.16	Comparison of joint angles and velocities for upstairs movement with step size $\Delta x = 0.4m$ . . . . .	35
4.17	Intermediate stepping poses for upstairs movement with optimized trajectory . . . .	36
4.18	Comparison of height trajectories for downstairs movement with step size $\Delta x = 0.4m$	37
4.19	Comparison of joint angles and velocities for downstairs movement with step size $\Delta x = 0.4m$ . . . . .	37
4.20	Intermediate stepping poses for downstairs movement with optimized trajectory . .	38
4.21	Changed input trajectory $z_{foot}$ for upstairs step with $\Delta z = 0.1m$ . . . . .	39
4.22	Cost function scan with $t_{high} = 0.5s$ for two upstairs steps with $\Delta z = 0.1m$ . . . . .	40
4.23	Cost function scan with $t_{high} = 0.4s$ for two upstairs steps with $\Delta z = 0.1m$ . . . . .	40
4.24	Poor initial solution in step three leads to bad performance of optimization result for preview period of $n = 4$ . . . . .	41
A.1	Foot trajectory in z-direction for downstairs with $\Delta z = -0.1$ . . . . .	44
A.2	Foot trajectories in z-direction for even walking . . . . .	45

# Glossary

**3D-LIPM** Three-Dimensional Linear Inverted Pendulum Mode.

**CoM** Center of Mass.

**CoP** Center of Pressure.

**CP** Capture Point.

**DCM** Divergent Component of Motion.

**EoM** Equation of Motion.

**LIPM** Linear Inverted Pendulum Model.

**MPC** Model Predictive Control.

**ODE** Ordinary Differential Equation.

**QP** Quadratic Programming.

**ZMP** Zero Moment Point.

# Chapter 1

## Introduction

### 1.1 Situation and Motivation

Robots have long arrived in our daily lives. Whether to produce what we buy and consume or to facilitate tasks in our day. Humanoid robots, however, are not yet freely roaming our world, like the lawnmower robot in the neighbors garden. Biped robots offer a great deal of advantages over wheeled robots. Their locomotion is based on human locomotion and they are therefore able to maneuver in human environment. This supposed advantage comes at the cost of high complexity of planning and control systems necessary to fully utilize the physical capabilities. This explains why biped humanoid robots are not yet able to operate outside of research facilities. Flexible walking in complex and uneven terrain still poses fundamental problems that are being researched around the world.

This thesis is part of the project "Walking in Uneven Terrain" <sup>1</sup> that is conducted at the Technical University of Munich in the Department of Mechanical Engineering. The Chair of Applied Mechanics tackles problems arising from locomotion in the real world in this project, using the biped robot *Lola* <sup>2</sup>. Challenges are to allow flexible and robust walking. The aim of flexible walking is to enable the humanoid robot to autonomously navigate in a previously unknown complex environment with obstacles and platforms or stairs. Another central requirement is to achieve these aims in real-time. Many improvements have been made to autonomously detect and avoid obstacles in a cluttered environment in real-time [10, 11, 46]. The work in this thesis is aimed at improving the ability to step onto platforms or stairs. Currently this cannot be achieved in a flexible way, manual tuning is necessary. A previous student's thesis explored the importance of alternative foot trajectories, namely making use of the toe joint, in descending stairs [40]. So far toe walking is not yet implemented on the humanoid robot *Lola* and can not be employed to improve walking in uneven terrain.

A different approach to achieve flexible stepping on and off of platforms or stairs is done in this thesis. The height of the Center of Mass (CoM) takes a central role in the planning and generation of the overall robot trajectories. So far the potential influence on achieving improved walking patterns by changing the vertical CoM trajectory has not been assessed on the humanoid *Lola*. This will be done in this thesis.

### 1.2 Concept

Research into variable CoM trajectories is numerous. An overview of existing approaches is given in chapter 2 together with a brief introduction to how the motion of a robot is planned during

---

<sup>1</sup><http://www.amm.mw.tum.de/en/research/current-projects/humanoid-robots/walkinguneventerrain/>

<sup>2</sup><http://www.amm.mw.tum.de/en/research/current-projects/humanoid-robots/lola/>



the so called pattern generation. The pattern generation system employed on the humanoid *Lola* allows to freely command a vertical CoM trajectory. In chapter 3 the approach of how to generate this trajectory is presented. The approach is a combination of different strategies already investigated by other researchers. Based on kinematic observations and conclusions a favorable trajectory is generated that is later subjected to numerical optimization. The performance of this approach is then assessed using a simulation environment in MATLAB. This is described in chapter 4. The thesis is concluded in chapter 5.

## Chapter 2

### Overview and Related Work

It is hard to get an extensive overview of existing work in the field of humanoid robotics. The amount of different approaches to the same problems leads to an ever increasing variety of solutions. This chapter provides a short insight to pattern generation in humanoid robots. Section 2.1 showcases pattern generation by presenting common methods and their implications for a variable Center of Mass (CoM) height. Section 2.2 explains why a vertical CoM variation is favorable and how it can be included in pattern generation.

#### 2.1 Pattern Generation

Pattern generation includes a multitude of tasks. Initially a set of high level input is given, such as step length, step time and a sequence of footsteps [24]. This high level data depends on information about the environment, the robots geometry and a possible operator [29]. The outcome of pattern generation is a set of reference trajectories, generally for the feet and the CoM. These trajectories are then used to derive the joint data for the robot.

One of the first tasks in pattern generation is to obtain the foot trajectories which are optimized with respect to energy consumption, collision and obstacle avoidance [3, 5, 11, 43]. These topics exceed the scope of this work and will not be covered further. The trajectories for both feet are assumed to be given.

In bipedal walking it is essential to ensure dynamic stability of the robot. In short dynamic stability means to avoid the robot tipping and falling over. The vast majority of pattern generation methods rely on a Zero Moment Point (ZMP) based approach [3, 4, 13, 14, 16, 21, 25, 27, 28, 29, 30, 31, 32, 33, 36, 37, 38, 39, 44]. This approach will be briefly presented in the following to give a basic idea. For further understanding please consult the respective literature.

Vukobratovic [45] first introduced the ZMP concept. Sardain [36] defines the ZMP as "the point on the ground where the tipping moment acting on the biped, due to gravity and inertia forces, equals zero, the tipping moment being defined as the component of the moment that is tangential to the supporting surface." To achieve dynamic balance the ZMP needs to be inside the convex hull of the robot's contact points at all times [3]. Be wary that the terms dynamic balance and dynamic stability are often incorrectly mixed in literature: dynamic balance can be correlated to the ZMP concept, however, achieving dynamic balance does not directly imply dynamic stability [3, 41].

For a given sequence of footsteps the ZMP trajectory can be planned within the respective support polygon which will later be used to ensure balance. There are multiple solutions for choosing a

favorable ZMP trajectory with different optimization goals, like a reduction of CoM velocities or contact forces [3]. These methods will not be examined further in this work.

In order to be able to compute all joint trajectories of the humanoid robot by inverse kinematics, foot trajectories and hip trajectories need to be determined [35]. A very common approach in bipedal robotics is to derive the CoM trajectories, and thereby ultimately the hip trajectories, from the governing Equation of Motions (EoMs) while ensuring balance in a ZMP based approach [16]. The formerly obtained ZMP trajectory can be regarded as a control system reference, whereas the CoM trajectories are the system output.

In order to obtain this control law a multitude of underlying models have been derived. They differ in complexity, accuracy and way of finding a mathematical solution. Furthermore different control methods are deployed. This leads to a wide variety of approaches with a similar base. In the following some of these approaches are discussed without a claim of completeness. The motivation of this overview is to point out the implications for the height of the CoM in different concepts. These implications are discussed further in Section 2.2.

An important milestone of a ZMP based approach in bipedal robots was the application of preview control to the ZMP [16]. Kajita et al. introduced a simplified version of the popular Three-Dimensional Linear Inverted Pendulum Mode (3D-LIPM) to model the walking movement and combine it with the ZMP concept [17]. The equations of the 3D-LIPM can be derived from the conservation of linear and angular momentum (2.1) (2.2) like it is done in [4].

$$m\ddot{\mathbf{r}}_{CoM} = \mathbf{F} + m\mathbf{g} \quad (2.1)$$

$$\dot{\mathbf{L}}^{CoM} = \mathbf{T} - \mathbf{r}_{CoM} \times \mathbf{F} \quad (2.2)$$

The vectors  $\ddot{\mathbf{r}}_{CoM}$  and  $\mathbf{r}_{CoM}$  stand for the CoM acceleration and position respectively. The vector  $\mathbf{g}$  denotes the gravity,  $\mathbf{L}^{CoM}$  is the angular momentum with respect to the CoM,  $m$  is the mass of the robot and  $\mathbf{F}$  and  $\mathbf{T}$  are the total reaction force and torque respectively, applied to the stance foot of the robot. Both are nonlinear equations. To obtain the 3D-LIPM equations it is assumed that the change of angular momentum is negligible:  $\mathbf{L}^{CoM} \approx const.$  Under this assumption the simplified EoM for the CoM are obtained (2.3) (2.4).

$$mz_{CoM}\ddot{x}_{CoM} - mx_{CoM}(\ddot{z}_{CoM} + g) = T_x \quad (2.3)$$

$$mz_{CoM}\ddot{y}_{CoM} - my_{CoM}(\ddot{z}_{CoM} + g) = -T_y \quad (2.4)$$

In order to decouple these equations Kajita et al. assume constant height of the CoM:

$$z_{CoM} = z_c = const. \quad (2.5)$$

This leads to the equations of the cart-table model (2.6)(2.7)[16]. Here  $z_c$  denotes the constant reference height of the CoM,  $p_x$  and  $p_y$  are the coordinates of the ZMP to be tracked.

$$x_{CoM} - \frac{z_c}{g}\ddot{x}_{CoM} = p_x \quad (2.6)$$

$$y_{CoM} - \frac{z_c}{g} \ddot{y}_{CoM} = p_y \quad (2.7)$$

These equations are decoupled linear Ordinary Differential Equations (ODEs) and can therefore even be solved analytically and with little computational effort. This allows for feasible and smooth CoM trajectories [3]. Many implementations employ the cart-table model and assume a constant CoM height [16, 22, 27, 30, 31].

The nonlinearity in the governing EoMs, allowing a variable CoM height, pose difficulties in pattern generation. A high computational effort is necessary to solve these equations numerically. Therefore humanoids are still limited concerning usage of variable CoM height trajectories in real-time [44]. In Section 2.2 implementations with a variable CoM height are discussed.

## 2.2 Variable Center of Mass (CoM) Height

As computational power constantly rises, more and more complex tasks can be achieved in humanoids. This leads to the exploration of formerly untouched problems. In recent years this lead to an increasing amount of researchers exploring the possibilities and caveats of a variable CoM height. The variety of different approaches, however, shows that "online generation of biped walking motions in three dimensions [...] to introduce some desired vertical motion of the body, is still largely an open problem in humanoid robotics today", as Brasseur et al. state it [2].

### 2.2.1 Motivation

Enabling this vertical motion brings several advantages to humanoid walking. The arising complexity of tasks necessitates making use of these advantages. One important motivation to allow variable CoM height is to achieve a higher efficiency by more human-like walking [9, 23, 26]. The lower energy consumption also yields reduced loads and torques [9, 22, 23, 25].

Another major advantage is a greater kinematic flexibility. This includes larger possible strides [23], improved maneuverability on stairs [7, 15, 33] and in general on uneven terrain [13, 29, 47]. Kinematic constraints like the existence of the inverse solution, joint limits and the knee singularity can be avoided with greater ease by allowing an adoptable CoM height [23].

The higher accuracy of more sophisticated models accounting for the coupling of the governing EoMs additionally leads to a reduced ZMP error and therefore improves the balance [25, 33]. Chevallereau and Aoustin even show that vertical oscillations of the CoM induce a self stabilization [6].

### 2.2.2 Modeling Approaches

Regardless of all possible advantages of a variable CoM height the problem persists that the nonlinear EoMs are still today numerically expensive to solve [44]. This difficulty is resolved in different ways. To limit the scope, methods not suitable for real-time execution are not considered here [14, 20, 38]. Hereafter I present various concepts, without a claim of completeness. Many actual implementations combine some of these methods together. Here, however, the approaches will be presented briefly and isolated.

One way to enable a variable CoM height is "assuming that the small change of the torso height does not affect the dynamic balance" [29]. The dynamic balance is then obtained by using simpler models like Linear Inverted Pendulum Model (LIPM). The deviation of the torso or CoM height from the constant reference height is then modeled as a disturbance. Li et al. analyzes the resulting error to the ZMP control [22]. Accordingly the relative effect of the height variation  $\Delta z/z_c$  on the error is small compared to a variation in the acceleration  $\Delta \ddot{z}/g$ . The use of smooth CoM trajectories in z-direction therefore reduces the error in this approach [22, 33]. Li et al. confirm even walking with an improved efficiency in a dynamic simulation using this method [22]. Park et al. provide experimental results of enabling a bipedal robot to walk upstairs by adjusting the CoM height [33]. Also in [29] the application of this assumption proves suitable for a full-size humanoid robot to walk over platforms in experiments.

In a different approach Lack assumes a known reference CoM height that is being followed perfectly by the robot [21]. The nonlinear governing EoMs hereby become linear with respect to the Center of Pressure (CoP) position and the spin angular momentum [9]. The author uses these simplifications to obtain an efficient solution of the nonlinear inverted pendulum dynamics by applying Model Predictive Control (MPC) and Quadratic Programming (QP). The results are, however, not backed by any dynamic simulations nor experiments. Through the application of MPC and QP also Van Heerden achieves real-time performance while allowing a variable CoM height [44]. The author showed the feasibility of his approach in simulations.

Another popular solution is to formulate surface constraints within which the nonlinear problem can be simplified. Both [25] and [48] derive a parametric surface representation to confine the CoM trajectory. Morisawa et al. [25] express the CoM motion as a parametric surface described by a spline surface. This leads to a parametric reduction to two functions of time. Consequentially the calculation of the solution is simplified. A numerical solution is obtained using Newton's method. Both simulation and experiment confirm stable stair walking, however, online applicability is not mentioned. Zhao and Sentis [48] reduce the dimensionality of the equations by introducing non planar surfaces. These are piecewise linear surfaces that confine the 3D movement of the CoM. This approach yields decoupled equations for the saggital and lateral planes. The equations are solved using numerical integration. The results are not validated neither in simulation nor in experiment, merely motion capturing is used to validate the planner.

A relatively new theory, the so called Divergent Component of Motion (DCM) is applied in humanoid robotics with the aim to allow the solution of more complex models while accounting for a variable CoM height [8, 15, 41, 42]. The terms Capture Point (CP) [34] and extrapolated center of mass [12] are also used synonymously to DCM. The CoM dynamics can be separated into a converging and diverging part and therefore stable and unstable components [42]. Originally derived from the LIPM the control in this approach focuses on the diverging part of the dynamics, since the stable part will converge also without control [42]. Both Hopkins et al. [15] and Takenaka et al. [42] prove the feasibility of their approach in experiments.

Finally the method incorporated with the humanoid robot *Lola* allowing for variable CoM height is the so called collocation method [4]. In general this approach numerically solves (partial) differential equations by finding a set of functions that satisfy the governing equations at a finite amount of points. In the method described by Buschmann cubic splines are used to approximate the nonlinear EoMs that describe a three point mass system.

$$\begin{aligned}
 m_b z_b \ddot{y}_b - m_b y_b (\ddot{z}_b + g) = & -T_x \\
 & + m_l y_{l1} (\ddot{z}_{l1} + g) - m_l z_{l1} \ddot{y}_{l1} \\
 & + m_l y_{l2} (\ddot{z}_{l2} + g) - m_l z_{l2} \ddot{y}_{l2}
 \end{aligned} \tag{2.8}$$

The indexes  $b$ ,  $l1$  and  $l2$  denote respectively the three different mass points for the body and both legs. By solving this equation via spline collocation instead of finite difference method the order of the problem can be reduced by magnitudes. The nonlinear equation (2.8) can hence be solved in real-time to allow arbitrary CoM height trajectories.

### 2.2.3 Trajectory Design

Numerous approaches to design the CoM height reference trajectory exist in literature. Different strategies are applied, ranging from heuristics derived from human walking to optimization problem formulations. In the following the terms CoM height, torso height and hip height will be used to describe the general concept of vertical motion of the body. In order to provide a better overview, the approaches are categorized, however, please note that the categories are not mutually exclusive.

#### Heuristic

Many vertical CoM trajectories are generated in a heuristic manner. Both Chevallereau et al. and Li et al. model the vertical CoM motion as a cosine oscillation around an average height  $z_0$  similarly to what can be observed in humans [6, 23]. In both implementations the wavelength corresponds to the step length and the cosine is a function of the horizontal CoM position. Li et al. correlate motion along the  $z$  axis and the  $x$  axis. They emphasize the usage of a sinusoidal function of position rather than time to avoid "a distorted sinusoidal pattern in the Cartesian space, as the horizontal velocity  $\dot{x}_{hip}$  is not constant". Chevallereau et al. additionally assume a decoupled dependency of motion along the  $z$  axis with the lateral CoM position (2.9). While both works show the advantages of enabling vertical oscillations in even walking, the methods do not consider uneven terrain.

$$z_{com} = z_0 + f_x(\cos(x_{com})) + f_y(\cos(y_{com})) \quad (2.9)$$

To allow climbing of stairs Park et al. generate the CoM trajectory in  $z$  direction as a 6th order polynomial [33]. They define boundary conditions and design parameters that are tuned in simulation to reduce the ZMP error. This yields an almost linear function which the authors used for simplicity. Drawbacks of this simplification are not examined.

Hong and Lee deploy varying trajectories in dual and single stance [13]. While a constant CoM height is assumed in single stance, the dual support phase is modeled through a cubic spline. This interpolation allows a shift to different CoM heights. The authors do not give a rationale as to how this solution is motivated apart from allowing a shift in height. The ability to stably walk in uneven terrain is shown in simulation.

#### Optimization

The basic approach in [37] consists of cosine functions of time for the variable hip height.

$$z_{com}(t) = \beta_0 + \beta_1 \cos\left(\frac{2\pi t}{L}\right) + \beta_2 \cos\left(\frac{4\pi t}{L}\right) \quad (2.10)$$

The periodic vertical motion is motivated yet again by the human hip height trajectory. The parameters  $L$  for the step period,  $\beta_0$  for the hip height offset,  $\beta_1$  and  $\beta_2$  for the cosine amplitudes are optimized. Subjected to a derivative-free stochastic optimization algorithm maximizing a

fitness function they are obtained in an offline calculation. The feasibility of the derived variable CoM height is shown in simulation for even walking. By comparing constant with variable height the authors show an improved performance using (2.10).

### Maximum Height

Miura et al. choose the waist height trajectory in a way that "straightens the leg as much as possible unless it exceeds the maximum distance  $L_{max}$ " [24]. Initially a constant CoM height is assumed and thereafter the leg lengths are computed. Whenever they exceed the maximum length  $L_{max}$  of a fully stretched leg, the waist is lowered to reduce the leg length. The resulting trajectory suffers from discontinuities at the transitions between dual and single stance phase. The authors therefore smooth the trajectory in an optimization with respect to a cost function constraining joint angles and velocities. The aim of the publication was to accurately imitate human-like motion and therefore the benefits of the variable CoM height are not explicitly mentioned other than successfully demonstrating even walking in an experiment.

In [18] Nishiwaki and Kagami perform the variation of the CoM height in a similar fashion. Their "basic strategy in this paper is keeping the torso as high as possible while satisfying the existence of the inverse kinematics solution and the limit of the knee joint velocity". The authors also include kinematic constraints in the generation of the torso height trajectory. They limit the vertical velocity and acceleration to obtain a smooth trajectory.

Their first step in the torso trajectory design process is the computation of the maximum kinematically feasible height. With the knowledge of the positions of right ankle joint  $(x_{ra}, y_{ra}, z_{ra})$  and right hip joint  $(x_{rh}, y_{rh})$  the maximum right hip height can be derived according to (2.11).  $L_{max}$  denotes the distance between hip and ankle joints with a fully stretched knee.

$$z_{rh,max} = z_{ra} + \sqrt{L_{max}^2 - (x_{rh} - x_{ra})^2 - (y_{rh} - y_{ra})^2} \quad (2.11)$$

Taking into account the left leg limits as well as torso posture, the overall maximum torso height allowing an inverse kinematics solution can be obtained.

Another limitation to the maximally feasible torso height is comprised of the knee joint velocity limit. The minimum of these two maximum heights serves as the basis for the height trajectory generation.

In the following the torso trajectory is designed considering both the maximally possible height and the vertical velocity and acceleration limits. In an iterative approach this is done by taking into account future height limits while staying within allowed velocity and acceleration ranges at all times. The result is a smooth trajectory that closely follows the maximum height. Nishiwaki and Kagami confirm the performance of the generated trajectory with experiments on a full-size humanoid robot.

In a newer publication Nishiwaki et al. formulate the torso height trajectory differently, yet with the same intention of "keeping the torso high" [29]. The approach was derived experimentally in simulations and real experiments. Cubic splines are used to interpolate between three heuristically defined support points per step sequence, at the start, middle and end. Each step sequence starts and ends in the middle of the dual support phase, when both feet are in contact with the ground. The interpolation points at the beginning and end of each step sequence are calculated so that the maximum torso height is closely approached without violating the knee singularity. The vertical velocity at those points is zero. The remaining middle control point assures a high torso position for when the swing leg is approximately under the torso. Similarly the height of the middle control point is derived by closely avoiding the maximum torso height.

The authors show the feasibility of the online trajectory generation method for uneven terrain in experiments.



## Chapter 3

# Vertical Center of Mass (CoM) Trajectory Generation

A new approach to generate the vertical CoM trajectory is presented in the following. The formerly employed trajectory lacks adaptability. Solely the set points at the beginning and end can be adapted, the transient behavior in between is not utilized. This limits the maneuverability especially in complex environments like the presence of stairs or platforms. So far it is only possible for *Lola* to ascend platforms by carefully tuning the trajectory manually. By replacing the current implementation with a more elaborate module it is hoped to achieve a greater flexibility in the kinematic maneuverability along with other advantages mentioned in 2.2.1.

In the scope of the overall pattern generation system the vertical CoM generation has only few interfaces to the rest of the system. The single output and therefore influence on the behavior of the system is the generated  $z_{CoM,ref}$  trajectory that serves as input to the module assuring dynamic balance. Inputs are limited as well, already due to the availability of information at this stage in the pattern generation process. The vertical CoM generation system only takes foot trajectories and high level stepping information, such as step length, step height and initial conditions as input.

Figure 3.1 visualizes the underlying idea of the system. The current reference trajectory is a constant curve, or in the case of ascending and descending a platform a simple smooth interpolation between start and end set points. The newly proposed method replaces this basic module in the overall pattern generation process. In contrast to the former method the new approach considers both high level walking information as well as task space trajectories such as the foot trajectories. This allows a better adaptability to the current scenario which becomes particularly important for climbing stairs and platforms. The trajectory generation is organized in a few submodules. First the maximally feasible hip height  $z_{max}$  is calculated based on geometric constraints as an upper bound to the trajectory being generated. Next an initial trajectory for the hip height is derived satisfying  $z_{max}$ . This initial solution is then subjected to optimization to obtain an even more favorable final solution for  $z_{CoM,ref}$ .

An important remark has to be made to distinguish between hip and CoM trajectory. The spline collocation method as described in [4] uses the notation of the CoM. As stated in equation (2.8) the CoM presentation is then split up to model three distributed masses in the two feet and the body. In the approach described in this chapter a trajectory for the hip height will be obtained. In order to ultimately include the derived method into the pattern generation system a transformation is necessary to obtain the corresponding CoM trajectory.

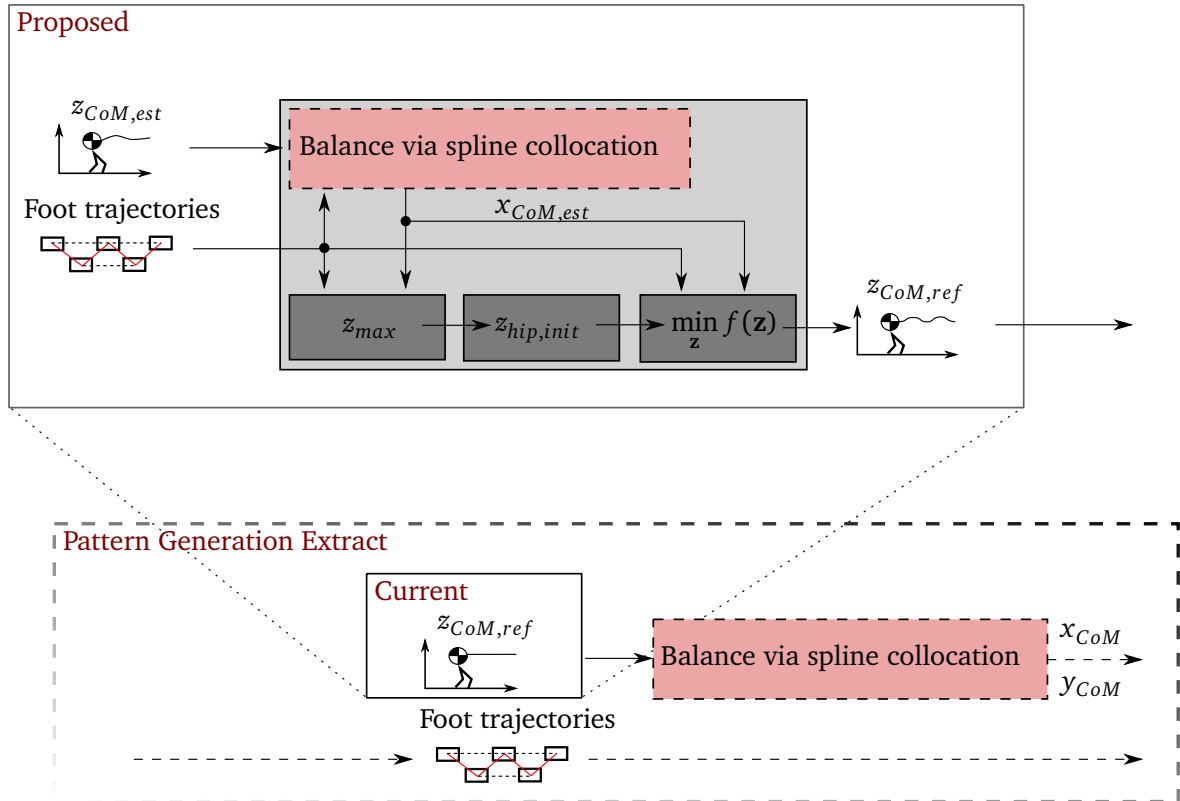


**Figure 3.1:** Overview of newly proposed trajectory generation system and section of pattern generation that gets replaced

### 3.1 Current Situation and General Assumptions

Before being able to derive the maximum hip height from geometric equations it is necessary to make an assumption that allows to integrate the proposed method into the overall pattern generation system. Figure 3.1 helps visualizing the alterations made.

The block "Pattern Generation Extract" shows a part of the overall system which is of interest in the scope of this work. Currently a quintic spline is used to obtain the vertical CoM trajectory. This polynomial is obtained by simply interpolating between start and end set point and is represented by the block "Current". This trajectory serves as a necessary input to the Boundary Value Problem (BVP) ensuring balance. The BVP is then solved by the spline collocation method. The outputs of the calculations are the horizontal CoM trajectories.

The newly proposed approach replacing the current vertical CoM reference is not able to use these outputs, as the block "Proposed" will replace the "Current" block, before the horizontal trajectories are obtained. They are, however, necessary to compute the maximum hip height and cost function for the optimization problem.

Consequently an iterative approach would be necessary to break this circular dependency. Instead elements similar to the current implementation are contained in the "Proposed" block. They serve as a first iteration which precede the new elements and provide them with an estimated  $x_{CoM,est}$ , similarly to how Nishiwaki and Kagami perform in [30]. In doing so, an error is introduced into the generation of the vertical CoM trajectory, since the optimized result and the estimate will most certainly not be equal.

The underlying assumption to justify the introduced error without reducing it via further iteration is that the change in the CoM height is a disturbance that does not affect dynamic balance of the robot [29]. Similarly in [30] Nishiwaki and Kagami state that "the effect of changing the torso

height to dynamics can be neglected" by limiting the maximum acceleration. Also Li et al. find in an error analysis that the error in the dynamic solution is determined by the error in the second derivative of the torso height rather than the error in the height itself [22]. Consequently it is assumed that smooth initial and final trajectories have a limited effect on the solution for the horizontal CoM trajectories. Please note that the dynamic balance will not be affected at all in this approach because the horizontal CoM trajectories are only used internally in the newly proposed module and will be recalculated with  $z_{CoM,ref}$  as before. The only source of concern is that the error  $e_x = x_{CoM,est} - x_{CoM}$  could have a possible but limited effect on a change in  $z_{CoM,ref}$ , i.e. a no longer valid trajectory was used in the derivation of the vertical trajectory. This might result in a not optimal solution for  $z_{CoM,ref}$  or even the violation of kinematic limits, which can be assessed by also recalculating the kinematic limits.

## 3.2 Step Phase

The overall pattern generation system operates in the scope of the so called step phase. Every performed step gets planned in this entity. A step phase starts and ends in the middle of a dual-leg support phase, where both feet are in contact with the ground. During a step phase the swing leg advances to perform the step. The time, during which only the so called stance leg is in contact with the ground, is defined as the single stance phase. A further distinction could be made for the respective phases, which will be omitted here. Figure 3.2 illustrates a qualitative step sequence with the dashed poses qualifying as start and end poses. The following calculations will all be performed in an inertial coordinate system with origin in the current stance foot. For simplicity of the calculations the origin of this coordinate system will be moved to the ankle joint of the stance foot, as can be seen in figure 3.3. Step phases where the feet are either moved from a parallel stance or to a parallel stance are regarded as special cases and therefore not considered in the scope of this work. The step duration  $T = 1s$  is used in all of the calculations for the sake of convenience.

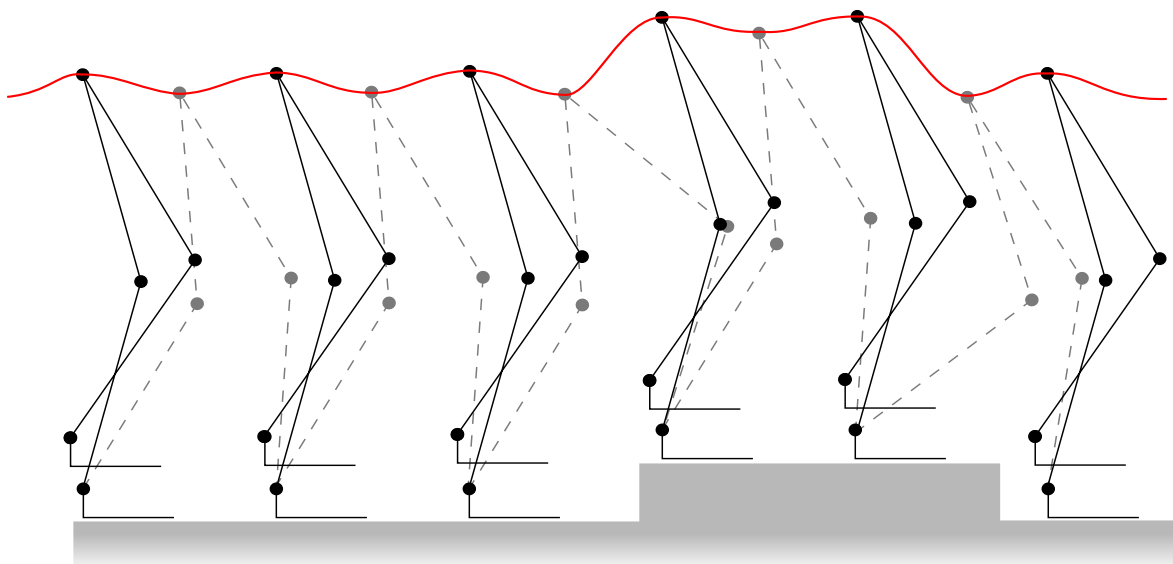
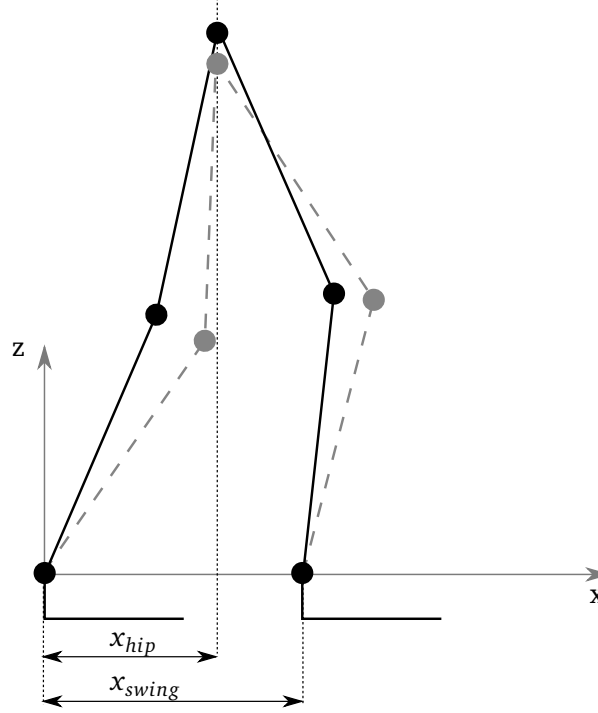


Figure 3.2: Step sequences

### 3.3 Maximum Hip Height

Maximum hip height refers to the height of the hip joint that is maximally feasible without violating geometric constraints. Ultimately the knee joint singularity prevents the humanoid robot from being able to walk with a fully stretched leg [18, 25, 29]. Similarly by a geometric constraint the distance between hip joint and ankle joint cannot be greater than the length of the fully stretched leg. This upper bound therefore is a valuable information in obtaining a vertical trajectory.



**Figure 3.3:** Kinematically feasible maximum height

According to the assumption made in 3.1 the maximum hip height is computed without changing the x-coordinate of the hip joint which correlates with the CoM. As assumed before the change in height does not affect the x-direction. This reflects the negligible effect on the dynamic balance. The maximum hip height can then be derived similarly to (2.11) with the following equations.

$$z_{sw,max} = z_{swing} + \sqrt{L_{max}^2 - (x_{hip} - x_{swing})^2} \quad (3.1)$$

$$z_{st,max} = z_{stance} + \sqrt{L_{max}^2 - (x_{hip} - x_{stance})^2} \quad (3.2)$$

$$z_{max} = \min(z_{sw,max}, z_{st,max}) \quad (3.3)$$

Figure 3.3 illustrates the distances used in these equations. The length  $L_{max}$  corresponds to the distance between ankle and hip joint for an almost fully stretched knee. Similarly to [18] the minimum knee angle is set to  $0.1[\text{rad}]$ .  $L_{max}$  can be derived as follows, where  $l_s = 0.43\text{m}$  is the length of the shank of Lola and  $l_t = 0.44\text{m}$  is the length of the thigh.

$$L_{max} = \sqrt{(l_s + l_t \cos(0.1))^2 + (l_t \sin(0.1))^2} \quad (3.4)$$

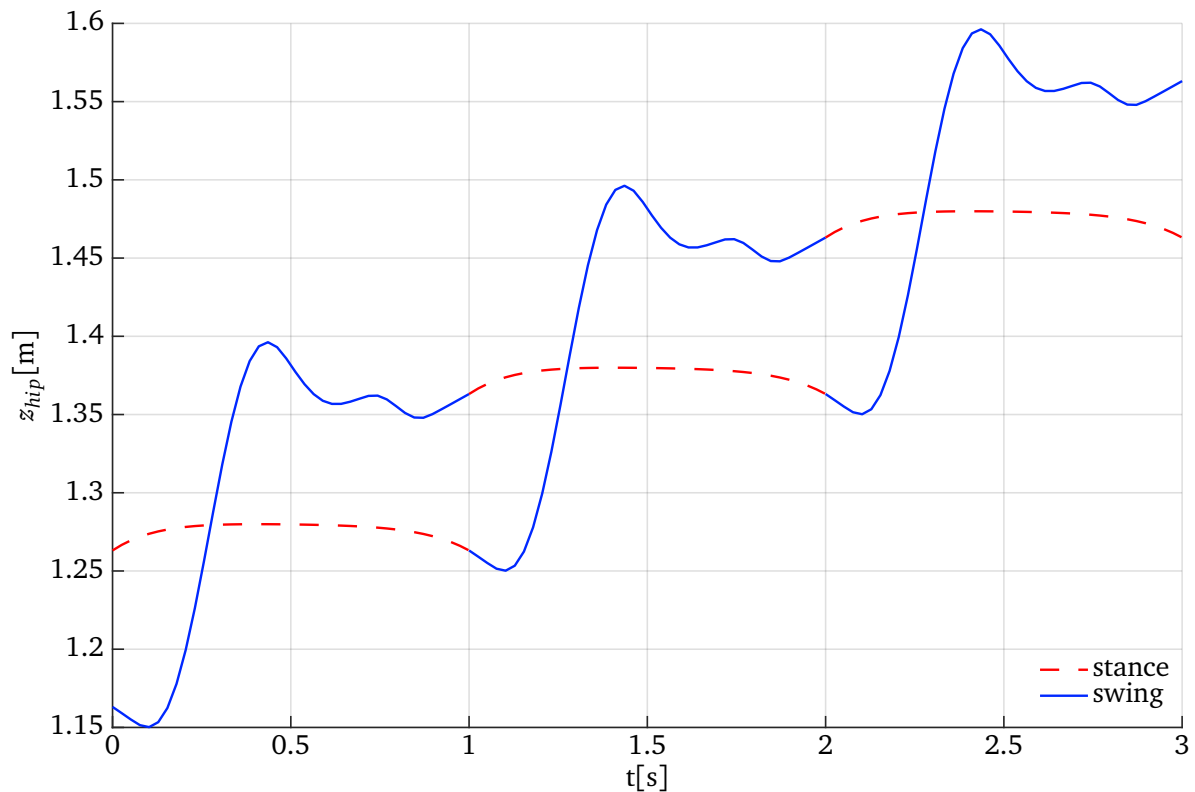


**Figure 3.4:** Maximum hip height for swing and stance leg for 3 steps upstairs with  $\Delta z = 0.1m$

Figure 3.4 shows the result for the maximum hip height during stair ascent. For the three steps performed it can be distinguished between the height derived from stance and swing leg. The maximum hip height for the stance leg varies only by the hip joint advancing with the torso. Mid stance the height barely changes at all, since the torso slowly advances above the foot. Towards the beginning and end of the step period the height reduces. The maximum hip height derived from the swing leg shows a greater variation. Initially the torso continues to move away from the swing leg, until the leg lifts off the ground and thereby reduces the distance to the hip joint. Eventually the swinging foot is closer to the hip joint yet again and the maximum hip height derived from the swing leg surpasses the stance leg calculation. According to (3.4) the lower boundary of the two curves makes up the overall maximum hip height. While the hip height stays below this reference, the knee will not be fully stretched.

## 3.4 Initial Hip Trajectory

### 3.4.1 Requirements

In order "to avoid excessive forces that could damage and/or destabilize the robot, connections should be  $C^2$ -smooth" for CoM trajectories [3]. As stated in 3.1 a smooth initial estimate for  $z_{CoM,init}$  limits the effect on the horizontal CoM trajectories. Based on these requirements for robot trajectories in general and the CoM height trajectory in particular a cubic spline representation is chosen. The current trajectory for the CoM height uses quintic polynomials. This parametrization also provides  $C^2$ -smooth trajectories. The drawback of this representation is, that the first and second derivative have to be known at the set points. A common assumption

for fully determining quintic splines therefore is, to set these two properties to zero at the set points. Both options are not desirable for the use in this approach. Cubic splines are by definition  $C^2$ -continuous at curve segment connections, i.e. the resulting curves are continuous up to the second derivative, without having to be specified. They are defined in 3.4.2.

The initial trajectory is required to be executed directly without optimization if need be. To be integrated in the real-time control of the robot there has to be an available valid solution at all times in case the optimization fails or an execution-time limit is reached. This necessitates a careful choice of the initial solution regarding violation of kinematic limits. These requirements are ensured by the proper choice of constraints introduced in 3.4.3.

### 3.4.2 Cubic Splines

Cubic splines are a popular choice when it comes to trajectories in robotics [3, 19, 29, 43]. The standard definition of cubic splines will be reviewed here briefly, corresponding to the notation used in [43].

A cubic spline interpolates a trajectory defined by a series of  $N$  support points with given locations  $z_k$  with their respective time points  $t_k$ :

$$(t_0, z_0), (t_1, z_1), \dots, (t_k, z_k), \dots, (t_{N-1}, z_{N-1}) \quad (3.5)$$

The trajectory consists of piecewise cubic polynomials interpolating between two consecutive waypoints and takes the following form:

$$f_k(t) = a_k + b_k(t - t_k) + c_k(t - t_k)^2 + d_k(t - t_k)^3, \quad k = 0, \dots, N - 2 \quad (3.6)$$

$$f(t) = \begin{cases} f_0(t) & \text{if } t_0 \leq t < t_1 \\ \vdots & \\ f_{N-2} & \text{if } t_{N-2} \leq t < t_{N-1} \end{cases} \quad (3.7)$$

There are  $4(N - 1)$  parameters  $a_k, b_k, c_k, d_k$  that have to be found to find a unique solution for  $f(t)$ . In order to enforce  $C^2$  continuity,  $3(N - 2)$  constraints are defined. They ensure continuity of positions, velocities and accelerations at the transition between neighboring cubic polynomials.

$$f_k(t_{k+1}) = f_{k+1}(t_{k+1}) \quad (3.8)$$

$$\dot{f}_k(t_{k+1}) = \dot{f}_{k+1}(t_{k+1}) \quad (3.9)$$

$$\ddot{f}_k(t_{k+1}) = \ddot{f}_{k+1}(t_{k+1}), \quad k = 0, \dots, N - 3 \quad (3.10)$$

In order to fully determine the cubic spline trajectory  $(N + 2)$  additional constraints need to be imposed. Commonly the support points mentioned in equation (3.5) are used in interpolation constraints, providing  $N$  additional constraints.

$$\begin{aligned} f_k(t_k) &= z_k, & k = 0, \dots, N - 2 \\ f_{N-2}(t_{N-1}) &= z_{N-1} \end{aligned} \quad (3.11)$$

A common approach to impose the remaining two constraints is to set so called natural boundaries. The curvature at the beginning and end of the trajectory is constrained to zero. This is

often done to facilitate solving the linear system of equations. The resulting matrix of dimension  $\mathbb{R}^{4(N-1) \times 4(N-1)}$  is tridiagonal hence the corresponding system of equations can be solved efficiently.

The initial solution for the hip height trajectory in this work, however, will neither involve natural boundaries, nor the interpolation constraints formulated in equation (3.11). The following subsection discusses the alternative formulation of  $(N + 2)$  equations to fully determine the cubic spline parameters.

### 3.4.3 Constraints and Support Points

The initial solution needs to qualify for serving as input to the subsequent steps in the pattern generation procedure. This and the observation that the optimization problem seems to suffer from local minima lead to a critical importance of choosing appropriate constraints and support points. Another key to a good initial solution is the adaptability to different stepping scenarios, i.e. even walking vs. stepping on or off a platform. Therefore a generic initial solution considers high level walking information like step size and height. The current choice for the missing  $(N + 2)$  constraints for the initial trajectory fuse together these aspects and observations and learnings made during the search for a feasible formulation.

#### Support Points

The amount of remaining impossible constraints  $(N + 2)$  is dependent on the amount of support points  $N$ . To be able to formulate the three initial conditions and allow three additional constraints four support points are needed per step period and need to be identified in at first. While the  $z$ -values of the support points are later subjected to optimization, the timings are not modified. Choosing the point in time is therefore crucial. In 3.5.1 an extension to consider future steps is introduced. This results in more support points and cubic spline segments. The following describes the procedure for a time horizon of just one considered step phase. In each additional step phase included the support points and constraints are identified respectively.

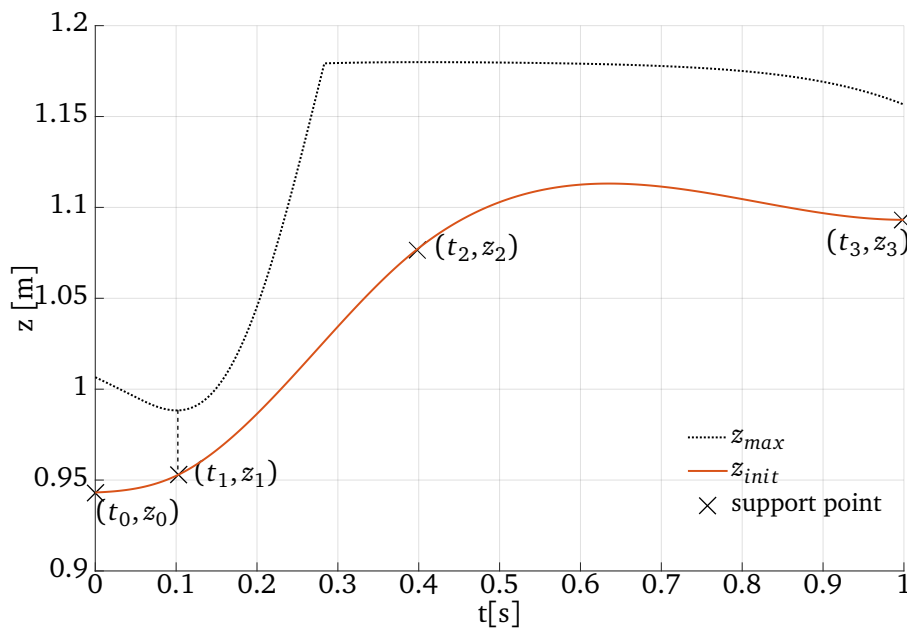


**Figure 3.5:** Choice of support points, here upstairs with  $\Delta z = 0.15m$

Figure 3.5 exemplarily shows the maximum height, a possible initial solution and the corresponding support points for a step with step height  $\Delta z = 0.1m$  and step time  $T = 1s$ . Two waypoints always lie at the beginning ( $t_0 = 0s$ ) and end ( $t_3 = 1s$ ) of each step period. Two additional support points need to be determined in between.

At the time  $t_1 = 0.1s$  the maximum height is minimal. This minimum appears both for stepping up and down platforms and results from the swing foot being lifted from the ground for upstairs or touching down for downstairs. By choosing this point in time both adaptability to the stepping situation and a consideration of the maximum height are achieved.

The second intermediate support point is chosen with human walking in mind. Figure 3.2 shows a qualitative step sequence. The torso is highest in an even walking cycle during single stance. This maximum occurs when the swing foot approximately passes the CoM [23]. To simplify the computation this is assumed to occur when the swing foot moved half way from initial to final position of the step period at  $t_2 = 0.4[s]$  in this case. Nishiwaki et al. achieve good results with choosing this mid swing moment as a control point for their torso height trajectory [29].

### Constraints

The next step is to formulate the missing  $(N + 2)$  constraints. Initially the trajectory is required to be smoothly connected to the motion concurrently being executed [3]. The initial conditions for the height trajectory then make up three constraints:

$$f_0(t_0) = z_0 \quad (3.12)$$

$$\dot{f}_0(t_0) = \dot{z}_0 \quad (3.13)$$

$$\ddot{f}_0(t_0) = \ddot{z}_0 \quad (3.14)$$

There are  $(N - 1)$  remaining constraints. For just one step phase with  $N = 4$  support points this results in three constraints. The constraint for the support point at  $t_1$  considers both high level step data and observations made during assessing the feasibility of the obtained initial solution. Looking at how the choice of a height trajectory affects the joint limits a critical region was identified. To force the hip height trajectory to follow the slope of the maximum height after the minimum, for upstairs movement a constraint for the derivative is imposed at the second support point. For downstairs movement the initial trajectory needs to follow the slope leading up to the minimum. The derivative in equation (3.15) is adopted to a ratio of difference in maximum hip height at the beginning and end of the step phase to the step time  $\Delta t_{step}$ . Thereby an adaptability to different step scenarios and maximum hip height is ensured.

$$\dot{f}_0(t_1) = \frac{z_{max}(t_3) - z_{max}(t_0)}{\Delta t_{step}} p_{tune} \quad (3.15)$$

The tuning parameter  $p_{tune}$  is a proportionality factor that is determined once. It allows to avoid an overshooting of the subsequent spline segments that could lead to a violation of the limit imposed by the maximum hip height. If  $p_{tune}$  is set too low the cubic spline does not follow the maximum hip height close enough. The result is a violation of the ankle joint angle, as can be seen in figure 3.6 on the right with  $p_{tune} = 0.2$ .

The last two constraints are both imposed to the support point at the end of the step phase  $t_3$ . Together they ensure a periodicity of the initial solution, especially important for when more than one step period is considered. Additionally the high level information about step height  $\Delta z$  is included. The derivative in equation 3.17 is imposed under the assumption only that the consecutive step phases are equal, i.e. one step follows another one. The initial velocity at the beginning of the first step phase is considered already optimal and the initial value for the following step is



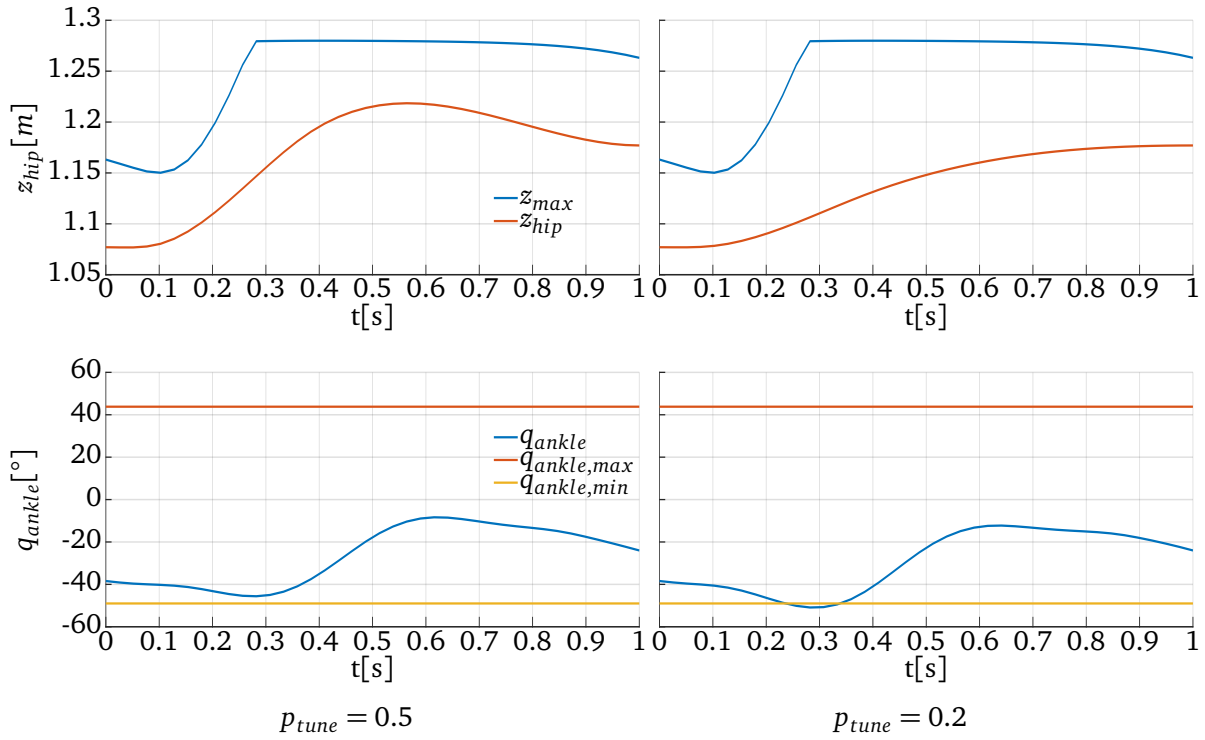


**Figure 3.6:** Choice of tuning parameter  $p_{tune}$

assumed to be equal because of periodicity.

$$f_2(t_3) = f_0(t_0) + \Delta z = z_0 + \Delta z \quad (3.16)$$

$$\dot{f}_2(t_3) = \dot{f}_0(t_0) = \dot{z}_0 \quad (3.17)$$

In total the equations (3.8)-(3.10) and (3.12)-(3.17) form a system of  $4(N-1)$  equations that fully determines the  $4(N-1)$  parameters  $a_k, b_k, c_k, d_k$  in (3.6). For a step sequence of  $n$  step phases considered this amounts to  $N = 3n + 1$  support points and therefore to a system of equations with dimension  $12n$ .

Figure 3.7 visualizes the constraints for the example of two steps upstairs with a step height of  $\Delta z = 0.05m$ . The total amount of  $N = 7$  support points in this case require  $N + 2 = 9$  constraints additionally to the smoothness constraints that are not displayed in the picture. The resulting initial solution can then be fully described by the support points obtained from this system of equations. These support points are then subjected to optimization, described in the following section as the optimization parameters  $\underline{z}$ .

### 3.5 Optimization

The overall aim for the new formulation of the torso height trajectory is to improve locomotion, in particular in uneven terrain. The optimization of the trajectory formulated in 3.4 takes an important role in reaching this goal. The parameters being optimized are the height values  $z_k$  of each support point but the first since it has to take the initial value  $z_0$ .

$$\begin{aligned} & \underset{\underline{z}}{\text{minimize}} && f(\underline{z}) \\ & \text{subject to} && z_k \leq z_{max,k}, \quad k = 1, \dots, N-1. \end{aligned} \quad (3.18)$$

The cost function  $f(\underline{z})$  is introduced in 3.5.2. The inequality constraint in (3.18) limits the optimization parameters not to exceed the maximum height.

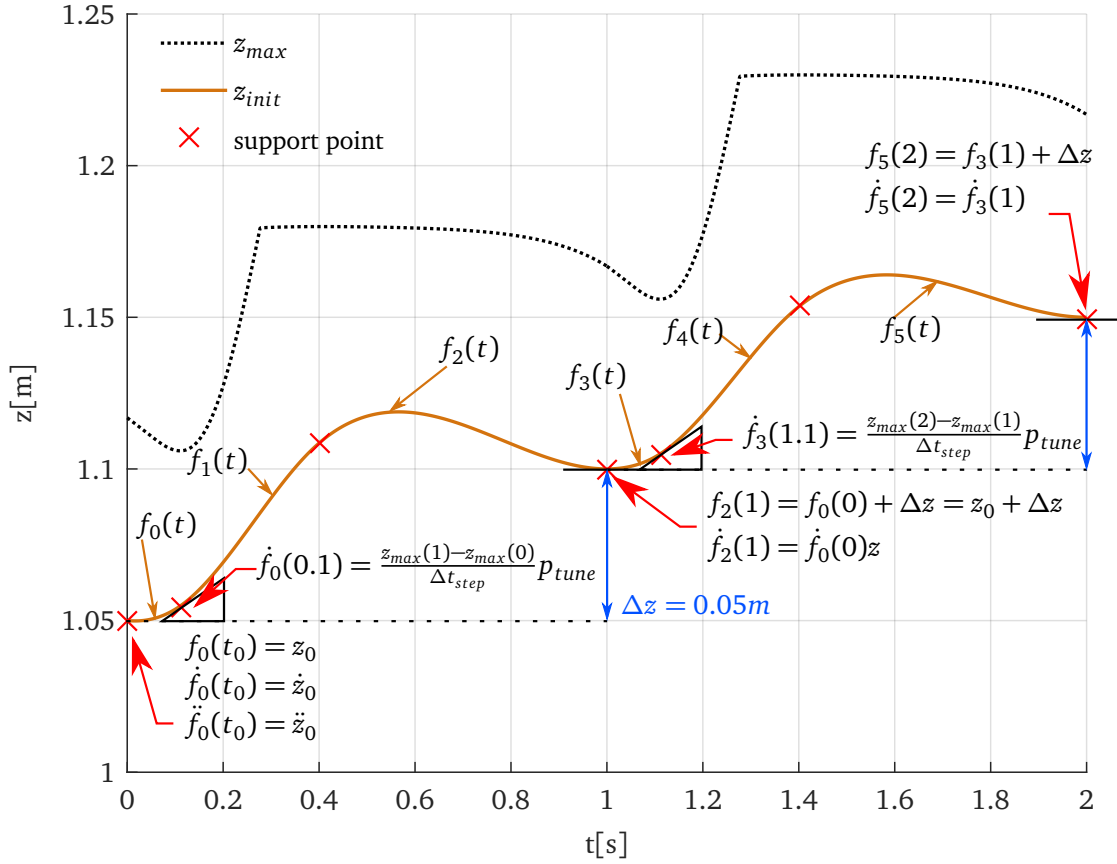


Figure 3.7: Initial conditions for upstairs movement with  $\Delta z = 0.05m$  for  $n = 2$  Steps

Another measure to improve the height trajectory is to include more than the upcoming step phase into the optimization.

### 3.5.1 Extended Time Horizon

This approach is motivated by Nishiwaki and Kagami, who elegantly include multiple future steps into the design of a torso height trajectory [30]. By broadening the time horizon to consider more than just the current step period, the authors are able to take into account future kinematic limits.

In this work  $n > 1$  steps are included into the trajectory generation process. The optimal amount of future steps to be embedded is assessed in 4.2. Every additional step that is incorporated leads to an increased dimension of the optimization problem. Figure 3.8 shows the result in the hip height for three different step sequences. For the times from  $t = 0$  to  $t = 3$  all three cases follow the same walking command, one even step and two steps upstairs. Starting at time  $t = 3s$  the walking commands for each case differ. The commands for the last two steps are either downstairs, upstairs or even walking. Including the knowledge about the following steps leads to the ability to improve the trajectory. In figure fig:horizonSteps this can be seen in the third step from  $t = 2s$  to  $t = 3s$  when the trajectories already differ although the command is still the same.

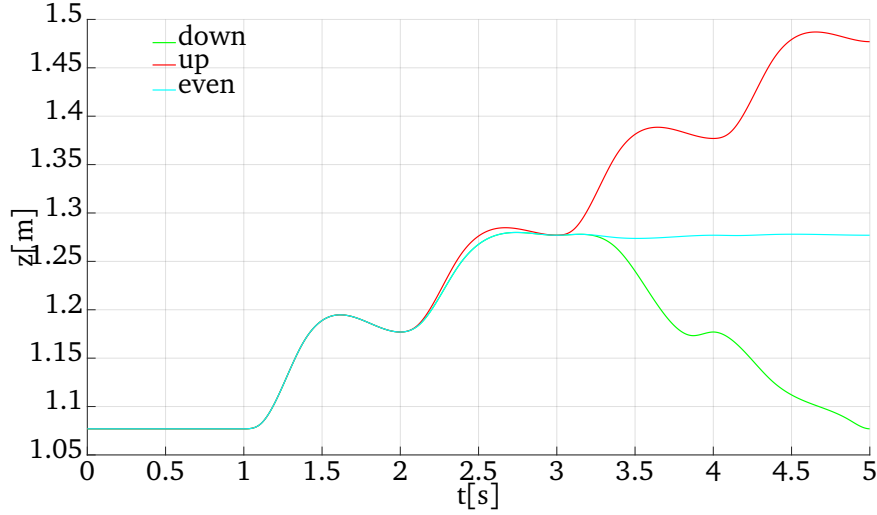


**Figure 3.8:** Differing step command after  $t = 3$  leads to change propagation to  $z_{hip}$  trajectories before  $t = 3$

### 3.5.2 Cost Function

The cost function  $f(\mathbf{z})$  in (3.18) is a scalar function of the optimization parameters.

$$f : \mathbb{R}^{N-1} \mapsto \mathbb{R}, \quad \mathbf{z} \in \mathbb{R}^{N-1} \quad (3.19)$$

The scalar cost function value penalizes undesired trajectories derived from the optimization parameters  $\mathbf{z}$  by higher return values. Conversely the evaluation of the cost function provides a way to measure how well the objectives are satisfied. A careful design of the cost function is necessary to allow a convergence to any optimal solution.

#### Objectives

Objectives for the optimization can be formulated in the cost function. Three essential goals are pursued here.

$$f(\mathbf{z}) = w_{vel} c_{vel}(\mathbf{z}) + w_{angle} c_{angle}(\mathbf{z}) + w_{z_{max}} c_{z_{max}}(\mathbf{z}) \quad (3.20)$$

In order to minimize the joint velocities  $c_{vel}(\mathbf{z})$  penalizes the square of joint velocities that result from a the current hip height. This is a common approach in robotics [19] and aims at an optimized energy consumption. The second term  $c_{angle}(\mathbf{z})$  seeks to ensure that the joint angle limits for knee and ankle are not violated. The violation of these kinematic constraints strongly increases the cost. Both joint angles and joint angle velocities are obtained using a simple 2D model introduced in 3.5.3. The third term  $c_{z_{max}}(\mathbf{z})$  is designed similarly to punish the violation of the maximum hip height. The factors  $w_i$  are the weighting factors that give a further design possibility for the cost function.

#### Calculation

The different costs  $c_i(\mathbf{z})$  in (3.20) are calculated in a discretized way. At first the cubic spline representation for the hip height trajectory is obtained from the optimization parameters, which initially represent the initial solution from section 3.4.

The joint velocity cost is then obtained using a simple 2D geometric model described in 3.5.3.

This model computes joint angles  $\mathbf{q}$  for ankle, knee and hip for a given configuration determined by hip and feet trajectories. The angle velocities  $\dot{\mathbf{q}}$  are then derived via finite central difference. Ultimately the joint velocity cost is computed as follows:

$$c_{vel}(\mathbf{z}) = \sum_i \dot{\mathbf{q}}(t_i)^T \dot{\mathbf{q}}(t_i) \quad (3.21)$$

Every robot joint has a limited working range. In this case limits for the ankle and knee joints are considered. In order to provide a differentiable cost function and to prevent the trajectory from approaching these limits  $c_{angle}(\mathbf{z})$  takes a value unequal to zero already in a certain range around the limits.

$$c_{angle}(\mathbf{z})_{i,j} = \begin{cases} c_j(-q_j(t_i) + (q_{j,min} + q_{j,margin}))^4 & \text{for } q_j < q_{j,min} + q_{j,margin} \\ 0 & \text{for } q_{j,min} + q_{j,margin} \leq q_j \leq q_{j,max} - q_{j,margin} \\ c_j(q_j(t_i) - (q_{j,max} - q_{j,margin}))^4 & \text{for } q_j > q_{j,max} - q_{j,margin} \end{cases} \quad (3.22)$$

The function (3.22) is exemplarily visualized in figure 3.9 for the ankle angle limits of  $q_{j,min} = -49^\circ$ ,  $q_{j,max} = 43.8^\circ$  and a margin value of  $0.1[rad]$ . Here  $q_j(t_i)$  depicts the angle  $j$  at time  $t_i$ , the factor  $c_j$  is used to scale the cost function to take the value 10 at the limit.

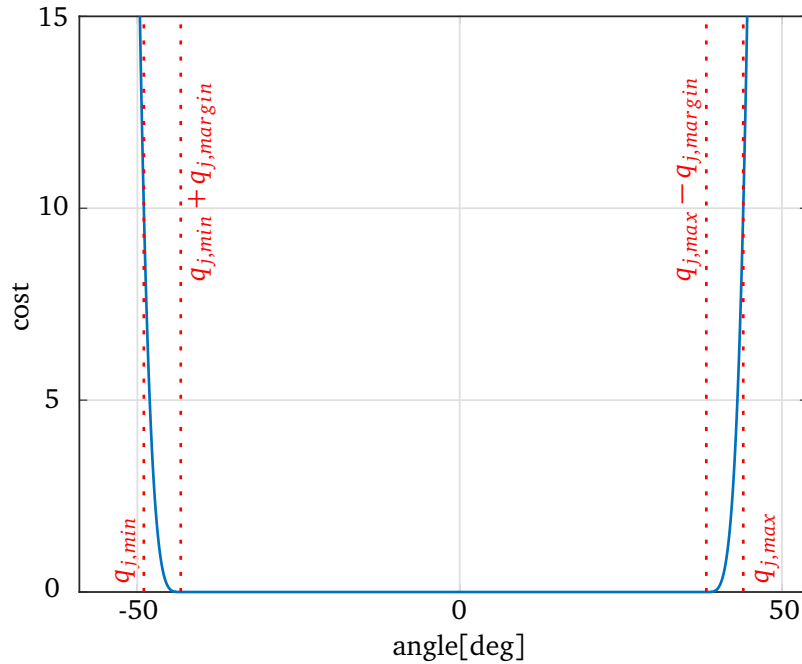


**Figure 3.9:** Angle limit cost function

The total cost for angle violations is obtained by summing over all considered discrete times  $t_i$  and all included joints  $q_j$ , in this case the two knee and the two ankle joints.

$$c_{angle}(\mathbf{z}) = \sum_j \sum_{t_i} c_{angle}(\mathbf{z})_{i,j} \quad \text{where } j \in [ankle_0, ankle_1, knee_0, knee_1] \quad (3.23)$$

The cost  $c_{z_{max}}(\mathbf{z})$  is obtained in a similar manner. The formerly computed maximum hip height  $z_{max}$  is the upper limit. The margin at what the cost function becomes active is  $z_{margin} = 0.02[m]$ .

### 3.5.3 Underlying Geometric Model

The simple geometric 2D model used for calculating the angles for the cost function is largely adopted from [40]. The lateral movement of the robot is omitted, as well as any rotations of the foot, meaning, the sole is always horizontal. The low detail of the model requires a later validation of the derived values with a more complex model. A low complexity of the model, however, is desirable, since the optimization process leads to a high number of function calls.

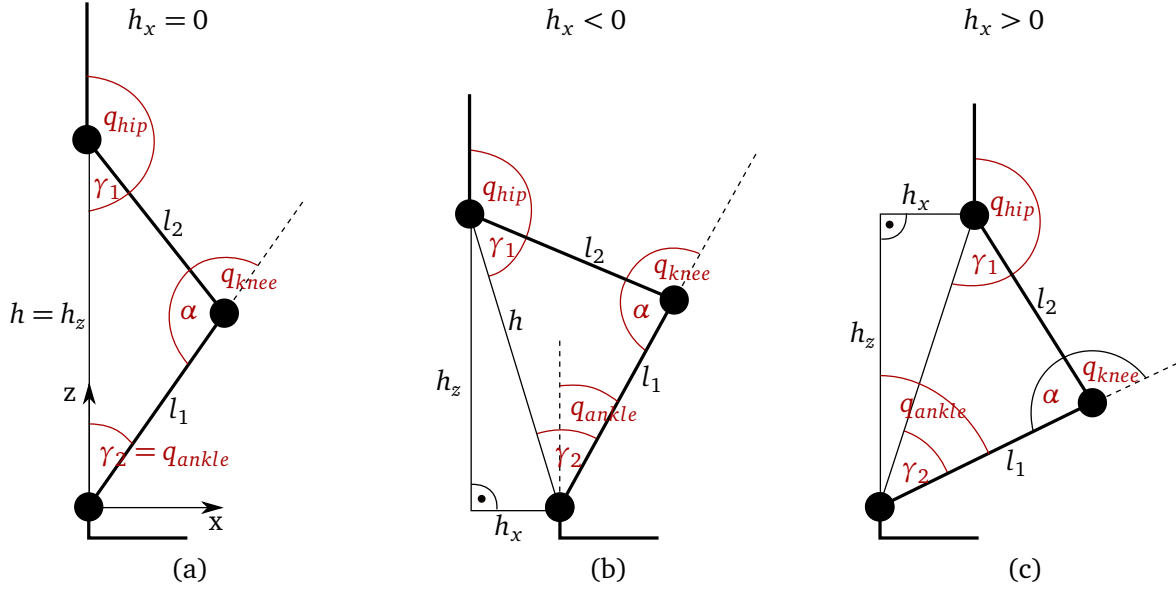


Figure 3.10: 2D geometric model for obtaining joint angles and velocities

Figure 3.10 shows 2D sketches of the robot in different postures. Together with the sign of  $h_x$ , the distance from the origin in the ankle joint to the hip joint projected in x direction, the derivation of the joint angles differs. The height difference between ankle joint and hip joint is denoted by  $h_z$ . The 2D distance between hip and ankle can then easily be derived via Pythagoras:  $h = \sqrt{h_x^2 + h_z^2}$ . With the knowledge of  $h$  one can easily obtain the angles in the triangle of the three leg joints.

$$\alpha = \text{acos}\left(\frac{l_1^2 + l_2^2 - h^2}{2l_1l_2}\right) \quad (3.24)$$

$$\gamma_1 = \text{acos}\left(\frac{h^2 + l_2^2 - l_1^2}{2hl_2}\right) \quad (3.25)$$

$$\gamma_2 = \text{acos}\left(\frac{l_1^2 + h^2 - l_2^2}{2l_1h}\right) \quad (3.26)$$

Differing with the sign of  $h_x$  the joint angles for the three leg joints can be derived from the angles in (3.24)-(3.26) and some basic trigonometry. The cases depicted in 3.10(a) and (b) can be combined in the following equations.

$$\begin{aligned} h_x \leq 0 \quad q_{ankle} &= 90^\circ - \gamma_2 - \text{acos}\left(\frac{h_x}{h}\right) \\ q_{knee} &= 180^\circ - \alpha \\ q_{hip} &= 180^\circ - \gamma_1 - \text{atan}\left(\left\|\frac{h_x}{h_z}\right\|\right) \end{aligned} \quad (3.27)$$

The equations corresponding to the conformation in 3.10(c) slightly differ.

$$\begin{aligned} h_x > 0 \quad q_{ankle} &= -\gamma_2 - a \cos\left(\frac{h_z}{h}\right) \\ q_{knee} &= 180^\circ - \alpha \\ q_{hip} &= 180^\circ - \gamma_1 + \operatorname{atan}\left(\left\|\frac{h_x}{h_z}\right\|\right) \end{aligned} \tag{3.28}$$

# Chapter 4

## Evaluation

### 4.1 Assumptions and Test Environment

The actual robot *Lola* is controlled in a framework implemented in C++ and running on a QNX based system. So far the implementation described in chapter 3 has not been integrated into the overall framework and therefore its performance will be evaluated in a MATLAB simulation. The simulation only provides the most basic interface that the generation of the vertical hip height needs, such as trajectories for the feet and horizontal Center of Mass (CoM). The simplified environment in this simulation and some assumptions made are described in the following section.

#### 4.1.1 Input Trajectories

One of the important assumptions to be made are the trajectories for the feet both in x- and z-direction which would normally be provided by the step planner. Additionally the trajectory for the CoM in x-direction is necessary. In the framework this trajectory is obtained from calculations to ensure dynamic balance via spline collocation.

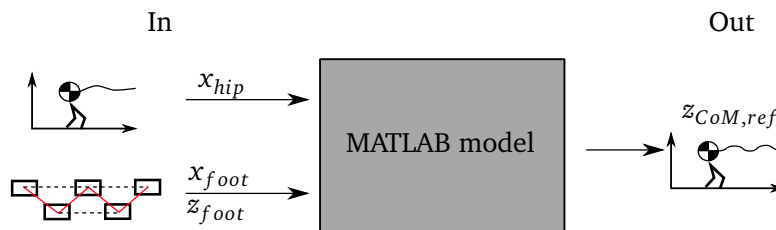
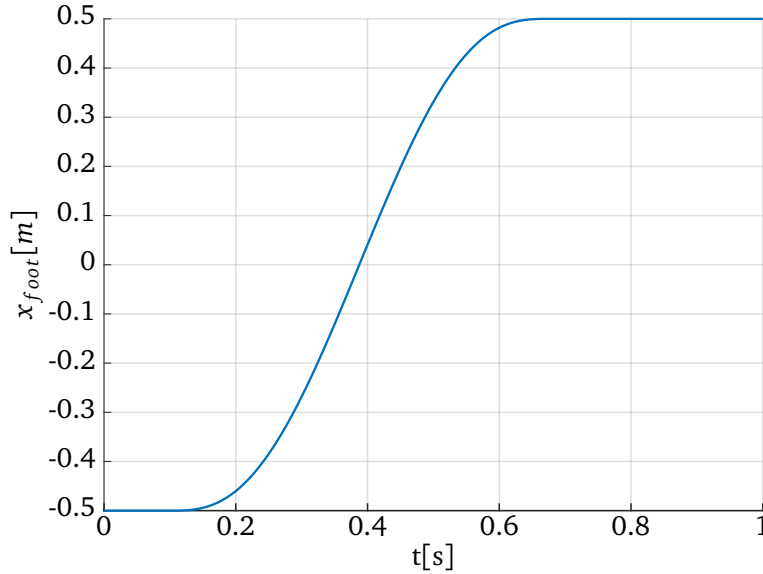


Figure 4.1: Input and output for MATLAB model

#### Foot Trajectory in x Direction

The foot trajectories in x are represented by quintic splines which are  $C^2$ -continuous. For each step phase there are three segments, the first and last during which the foot is at rest. During the second segment the foot is moved from start to end set point. As a result from the representation by quintic splines both velocity and acceleration at the set points can be defined to be zero. This is necessary to minimize the risk of slipping. The difficulty in choosing an appropriate trajectory are the timings. For the testing environment the timings were obtained empirically. Goals were to avoid collision with possible stairs and to roughly obtain a ratio of 40% swing to 60% stance phase similar to what can be observed on humans [1].



**Figure 4.2:** Foot trajectory in x-direction with  $\Delta x = 0.5m$

Figure 4.2 shows the resulting foot trajectory for a step length of  $\Delta x = 0.5m$ . Step length here refers to the distance between consecutive stance legs, meaning that the swing leg has to cover double the distance. Note that the illustrated trajectory describes the swing foot and is measured in the inertial coordinate system with origin in the stance foot.

### Foot Trajectory in z Direction

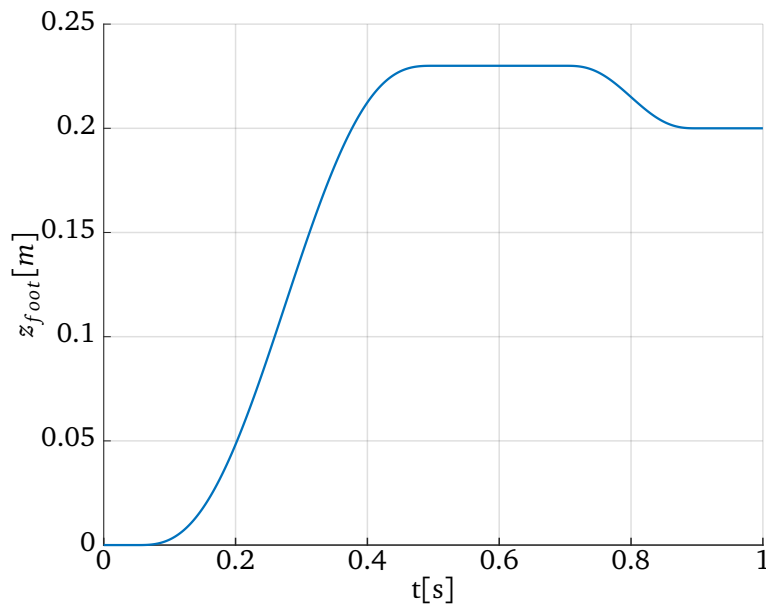
In z-direction the foot trajectories are represented by quintic splines as well. Similar reasoning applies, however, five segments are used per step phase. At the beginning and end there are resting segments, analog to the trajectory in x-direction. In z-direction the trajectory interpolates between three set points. The height of these set points depends on the overall movement. For ascending or descending a possible collision with the stairs has to be avoided. In the case of even walking it is only necessary to lift the foot to a predefined clearance distance away from the ground. Accordingly there are two transition segments. The first in order to move from the starting set point to the height at which the foot is also advancing in x-direction. In the second transition segment the foot returns to the final height where it will touch ground. In between those two transitions the foot is kept at a constant height. Also for the  $z_{foot}$  trajectory the timings are difficult to determine. Together with the trajectories in x-direction they were determined empirically. It was assured, that the foot is always lifted before advancing.

Figure 4.3 visualizes the resulting trajectory for upstairs walking with step height  $\Delta z = 0.1$ . Refer to figures A.2 and A.1 in the appendix for the trajectories obtained for even walking and downstairs walking respectively.

### Hip Trajectory in x Direction

As described in section 3.1 the horizontal trajectory for the CoM is necessary to derive the initial solution for the hip height. Similarly to what was stated at the beginning of chapter 3 the computations in MATLAB will be performed using hip coordinates rather than the CoM coordinates. A transformation between these two notations will be necessary prior to an integration into *Lola's* framework.





**Figure 4.3:** Foot trajectory in z-direction for upstairs with  $\Delta z = 0.1$

Hence, the hip trajectory would be ideally derived from the horizontal CoM solution that ensures dynamic balance. In this test environment a hip trajectory is derived based on some basic assumptions. Just as in the framework the curve is represented by cubic splines. This assures  $C^2$ -smoothness. The hip advances by one step length  $\Delta x$  per step phase. The initial position at the beginning of the step phase is assumed to be between the two supporting legs. The movement between the two set points is derived from observing the simulated balanced even walk of *Lola*. The torso and thereby the hip advances faster during the dual-leg support phase at the beginning and end of each step phase, to shift weight between supporting feet. In the single support phase the torso moves slowly above the stance foot. The resulting hip trajectory in x-direction is plotted in figure 4.4, together with the corresponding swing foot trajectory.

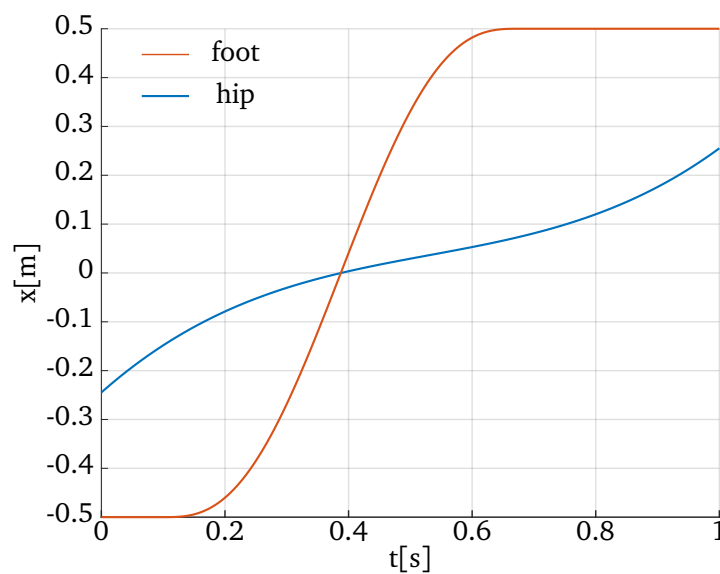


**Figure 4.4:** Foot and hip trajectory in x-direction

The plot shows a greater slope and thereby hip velocity in x-direction when the foot is not advancing.

### 4.1.2 Solver

The approach laid out in chapter 3 to generate the hip height trajectory is implemented using MATLAB. The optimization can therefore make use of the MATLAB Optimization Toolbox. For unconstrained minimization the function "fminunc" is offered. The gradient based "quasi-newton" algorithm provided within this toolbox is used to optimize the support points with respect to the cost function. The gradients are obtained numerically by forward finite differences. The implementation makes use of a cubic line search procedure and approximates the Hessian. For more detail consult the MATLAB documentation and the literature presented there<sup>1</sup>.

### 4.1.3 Shortcomings

It is not ideal to evaluate the performance of the vertical hip trajectory generation in the test environment described. The following discussion of results is done to allow some conclusions towards the planned implementation in the robot framework and to give ideas about possible difficulties. The findings and results should, however, best be read with the shortcomings in mind that the current evaluation suffers from:

#### Input Trajectories

The first problem stems from the choice of input trajectories to the system. The trajectories are generated with the real system in mind but they have not been validated with trajectories from the pattern generation system of *Lola's* control system.

#### Dynamic Effects

Dynamic effects can also not be covered in the scope of this analysis. Possibly some of the obtained trajectories are not feasible to be executed on the real robot. The dynamic limits, i.e. maximum accelerations, might prevent the robot to follow the proposed reference trajectory.

#### 2D

A general assumption made for sake of simplicity is the operation in two dimensions. Many of the calculations done in the proposed approach for a new vertical hip trajectory do not consider lateral robot movement. These simplifications need to be verified.

## 4.2 Optimal Amount of Predicted Steps

In order to obtain a better solution following steps can be included in the optimization. By doing so future occurring kinematic constraints can be anticipated beforehand. This can then have a retrospective effect on the trajectory of the current step phase. A number of simulations were performed varying the amount of steps included in the preview period. The results with differing step lengths  $\Delta x$  for even, upstairs and downstairs walking are visualized in figures 4.5, 4.7 and 4.8 respectively. The performance of the solution is measured in the cost function value obtained for a single fully optimized step phase according to section 3.5.2.

Figure 4.5 shows the performance of optimized hip trajectories in the case of even walking. The step length  $\Delta x$  was varied between  $\Delta x = 0.3$  and  $\Delta x = 0.6$ . For each step length five simulations

<sup>1</sup><http://mathworks.com/help/optim/ug/fminunc.html>

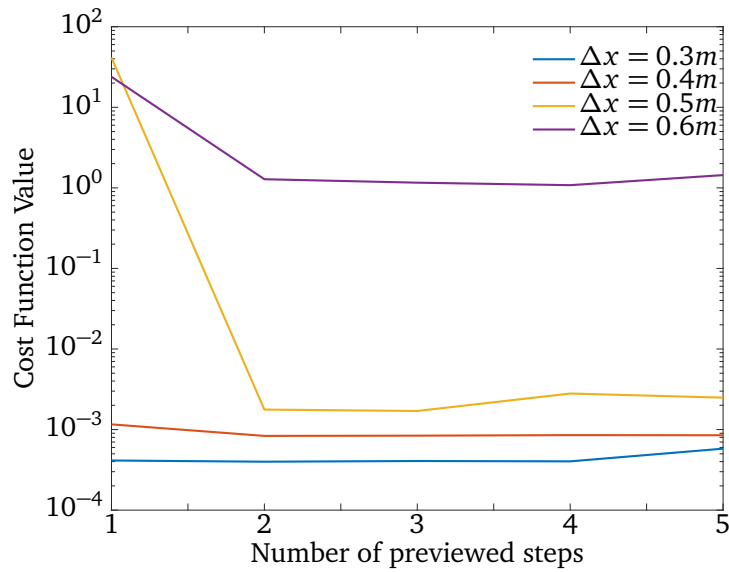


**Figure 4.5:** Performance of converged solution depending on steps considered in preview period for even walking

were performed with a preview period ranging from one to five steps. The five separate solutions for each step length are directly comparable since the step command is the same. The lower the cost function value is, the better the constraints defined in 3.5.2 are satisfied. For even walking and a small step length of 0.3m or 0.4m there is hardly any performance difference. For bigger steps the solutions improve strongly by considering two steps in the optimization as opposed to just one. Including more steps than two, however, only slightly changes the objective function value.

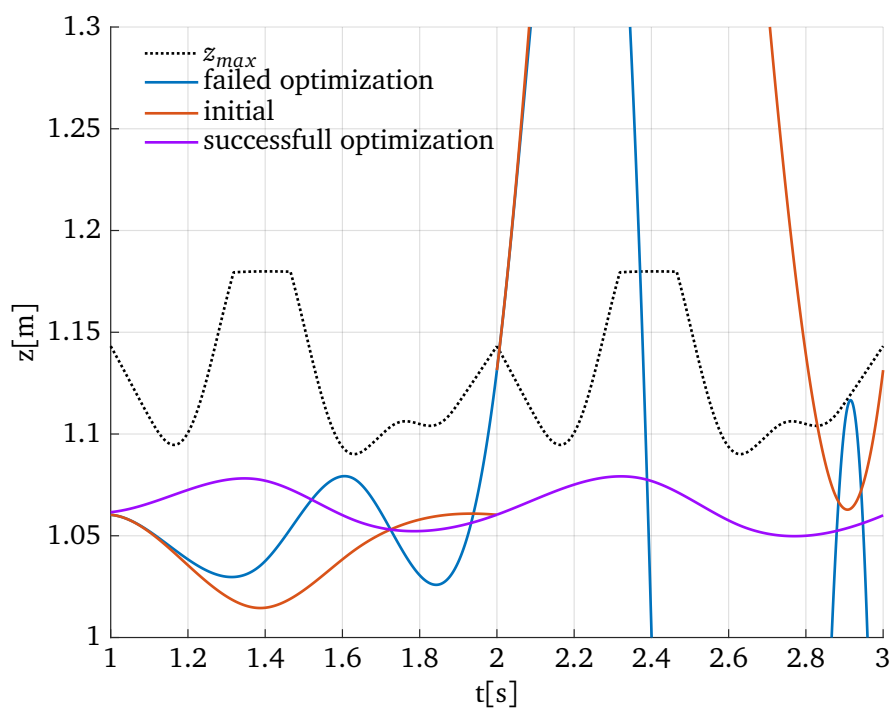


**Figure 4.6:** Trajectory generation failure for preview horizon of one step, displaying trajectories for two steps

Figure 4.6 shows why the optimization failed for a preview period of just one step in the case of

$\Delta x = 0.5m$  for even walking. The initial solution for the first step phase for  $1s \leq t < 2s$  is feasible and the optimized solution obtained is by means of the cost function a "good" solution. The resulting hip height trajectory would be feasible for the scope of the optimization which is in this case just the current step. The walking motion however continues and the following step starts with almost initially infeasible initial conditions. The  $C^2$ -continuity constraint dictates that the cubic spline in the second step phase needs to begin with the same position, velocity and acceleration that the preceding segment ended. In this case the spline parameters cannot be optimized to generate a feasible solution and the result is an oscillating cubic spline with high amplitudes. The trajectory for the successful optimization gives a reference of how the result looks if the following step is included into the optimization. Here the lack of knowledge about the following step becomes troublesome.

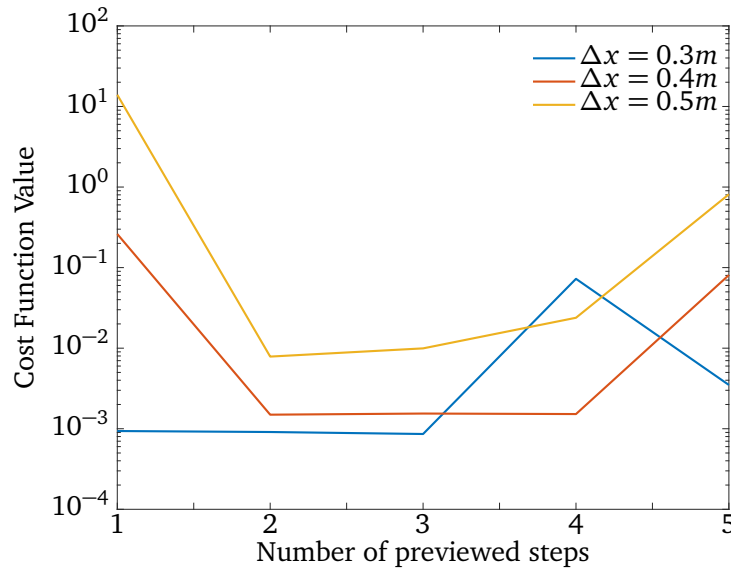


**Figure 4.7:** Performance of converged solution depending on steps considered in preview period for upstairs movement ( $\Delta z = 0.1m$ )

Some of these findings apply also for the upstairs scenario 4.7. While a good solution can be obtained with just one considered step for the smallest step size of  $\Delta x = 0.3m$ , an increased step size requires at least two. For two to four steps in the preview period the magnitude of the objective function value obtained is the same. The only exception occurs for four previewed steps and a step length of  $\Delta x = 0.3m$ . Whereas the solution yielded by the optimization is still feasible, i.e. does not violate any kinematic constraints, it is less favorable regarding the joint velocities. The objective function value for four previewed steps is by the order of one magnitude higher than that for three steps. Examining the initial trajectories in this particular case has showed that they were not already feasible and violated kinematic constraints. Generally the optimization procedure is able to yield a feasible solution also starting from an infeasible one. Including more steps when the initial trajectory per step is not sufficiently good amplifies this problem for each following step. This can lead to a deviation from the local minimum that the optimization is unable to recover. This is discussed further in section 4.4. For similar reasons the increase by an order of a magnitude occurs from four to five previewed steps for step lengths  $\Delta x = 0.4m$  and  $\Delta x = 0.5m$ .

From figure 4.8 it can be concluded that for downstairs movement the solutions of only previewing one step are also not favorable. Including two steps in the preview period brings great improvement again, regardless of the step length. Again the problem of a strong increase of the objective function value for a higher number of previewed steps is apparent.

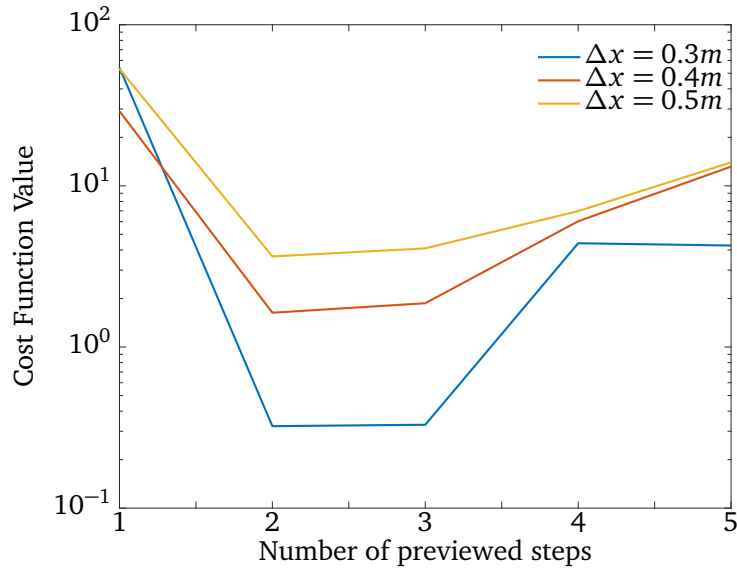


**Figure 4.8:** Performance of converged solution depending on steps considered in preview period for downstairs movement ( $\Delta z = -0.1m$ )

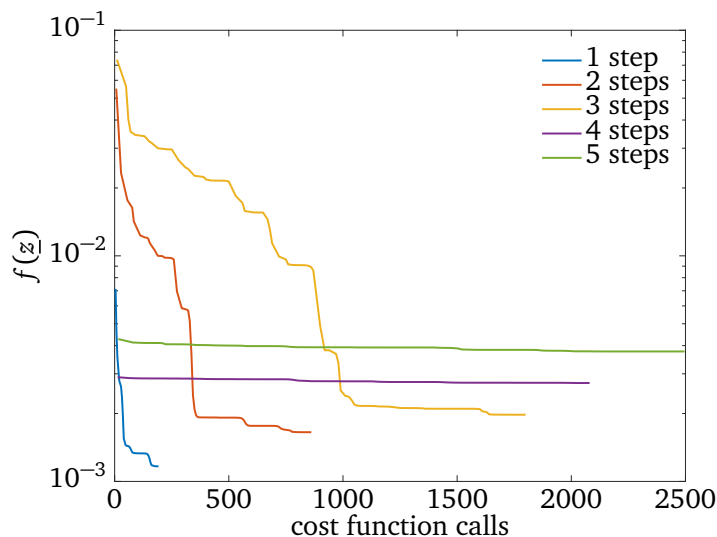


**Figure 4.9:** Convergence rate for even walking with  $\Delta x = 0.4m$

For the variation of step scenario and step length only using two or three previewed steps yields good solutions throughout the assessment. Another means for choosing how many following steps are best considered is the convergence behavior. Figures 4.9, 4.10 and 4.11 show the decrease of the objective function per function calls to the cost function for upstairs, even and downstairs movement respectively. The optimization time scales with the amount of function calls. It is therefore favorable to achieve convergence to a feasible solution for a low number of function calls. The setup that includes two previewed steps in the optimization in general converges faster and even up to double the speed as for three steps. The amount of future steps included in the optimization directly scales with the amount of optimization variables. For each additional step three additional support points are being optimized. Consequently more considered step phases lead to an increased optimization effort.

For the remainder of the evaluation a preview period of two steps into the future is chosen and re-

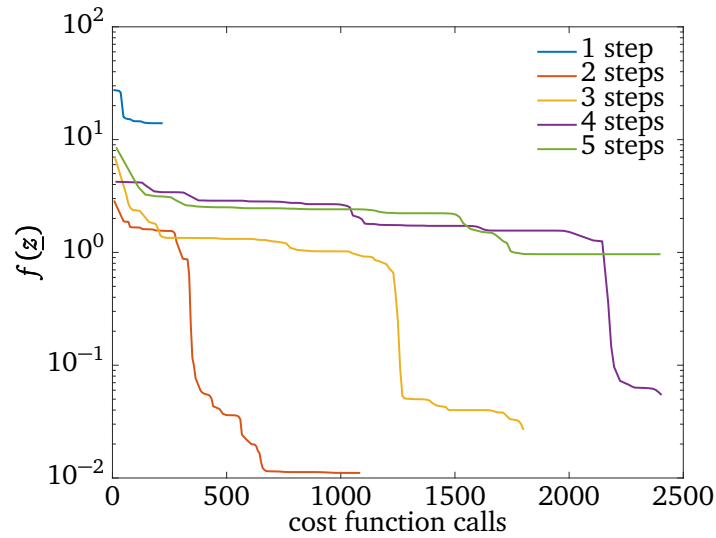


**Figure 4.10:** Convergence rate for upstairs scenario with  $\Delta x = 0.5m$

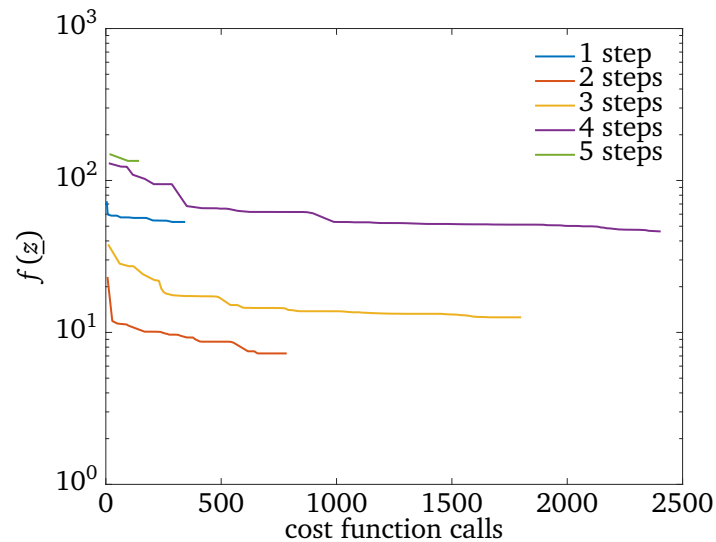


**Figure 4.11:** Convergence rate for downstairs scenario with  $\Delta x = 0.5m$

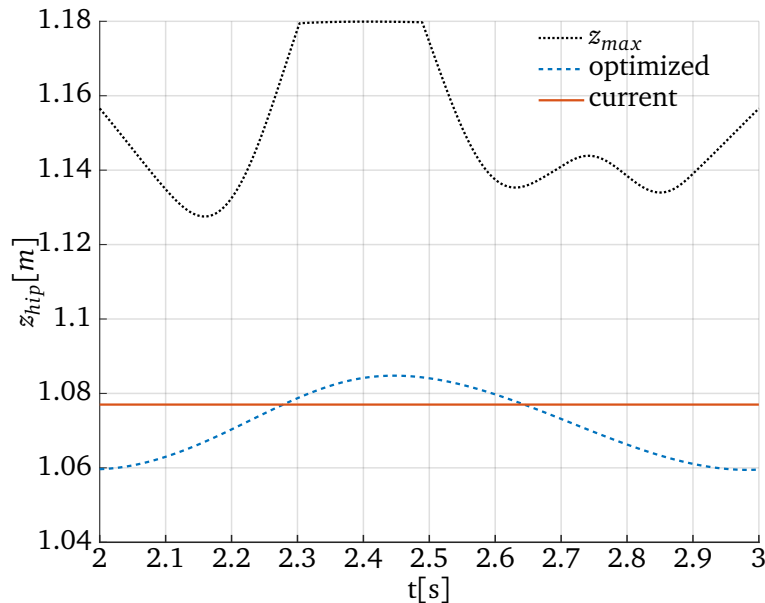
garded as optimal. While achieving an equally good solution as considering three steps the lower amount of optimization variables reduces the execution time for only considering two steps.

### 4.3 Comparison to Current Approach

The goal of the proposed approach is to kinematically improve movements by generating a more favorable hip height trajectory that avoids kinematic limits. In this section the new trajectory will be compared to the approach currently employed. The evaluation of the results is presented for different step scenarios.

### 4.3.1 Even Walking

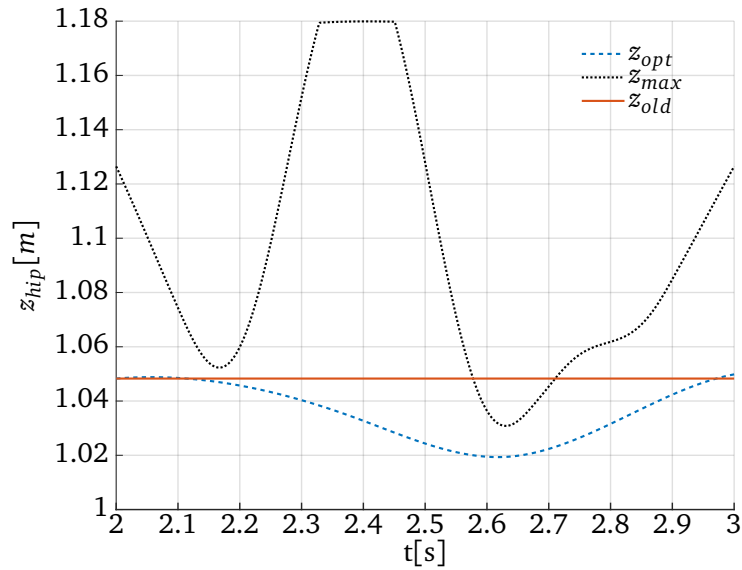
During even walking kinematic limits are not as problematic as they are during ascending or descending platforms or stairs. The height trajectory currently used is a constant height for even walking and this is sufficient in that case. It is not the main target of this new approach of generating a vertical hip height to improve the performance of even walking. Nevertheless the capabilities of doing so are assessed in the following.



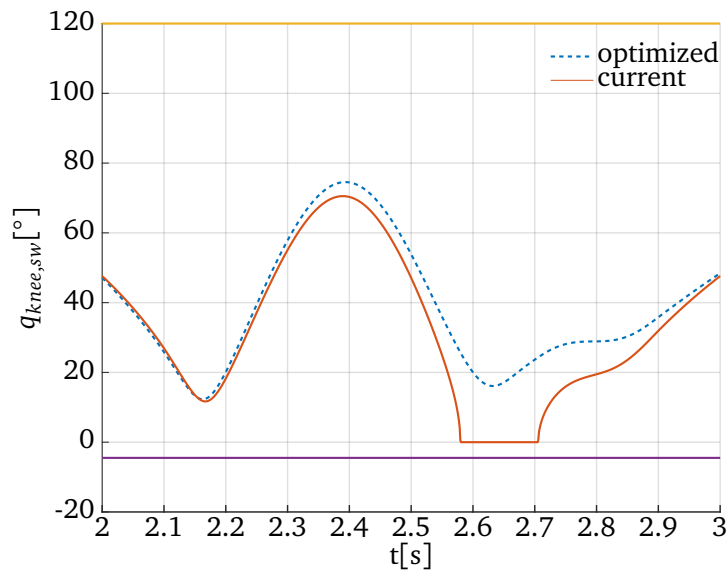
**Figure 4.12:** Comparison of height trajectories for step size  $\Delta x = 0.4m$

Figure 4.12 shows the the optimized and the current height trajectory for a step size of  $\Delta x = 0.4m$ . Kinematic limits that are represented by the maximum hip height are not near the constant hip height and therefore pose no problems. The obtained optimized solution takes a sinusoidal form varying around the constant height trajectory. The hip height is highest mid phase during the single stance phase. This is similar to what can be observed in humans. During the single stance phase the leg is stretched further to increase the height and reduce the load on the knee. It also holds true for robots that a reduced knee joint angle leads to lower torques, as Li et al. state in [23]. The dynamic effects of this new trajectory cannot be assessed in the scope of this simulation. In a dynamic simulation or experiments it could be analyzed if a reduction of about  $\Delta q_{knee} = -2^\circ$  leads to a notable improvement. In this particular scenario the difference between the constant height and the optimized height in terms of cost function value is rather small. The optimized trajectory achieves a value 5.39% lower than that of the constant height.

For larger step lengths the kinematic limits take on greater importance as can be seen in figure 4.13. In this particular scenario of a step length of  $\Delta x = 0.6m$  the maximum hip height is much lower. As a result the constant hip height even violates this constraint. The optimized trajectory, however, avoids the kinematic limit by lowering the hip height. The reason for this violation can be seen in figure 4.14. The currently employed constant height trajectory leads to a knee joint singularity for the swing leg. By using a lower hip height during the single stance phase the optimized trajectory avoids the knee singularity and remains at a sufficient distance to the knee angle limit. Therefore the proposed height trajectory generation method could also offer improvements to even walking in the case of long step lengths.



**Figure 4.13:** Comparison of height trajectories for step size  $\Delta x = 0.6m$



**Figure 4.14:** Comparison of knee joint angles of swing leg for step size  $\Delta x = 0.6m$

### 4.3.2 Upstairs

Ascending platforms or stairs flexibly is not possible using the current height trajectory. A manual tuning of parameters is necessary to achieve this task. Currently a quintic spline is employed to interpolate between the set points at beginning and end of the step phase, being  $\Delta z$  apart in height. This trajectory and the one obtained by optimization are plotted in figure 4.15. One observation from the plot is that the optimized curve during the single stance phase reaches a height of more than  $0.10m$  higher than the quintic spline, while staying within the bounds of the maximum hip height.

With the increased height the knee angle of the stance leg is more than halved at  $t = 2.5s$  as can be seen in figure 4.16. Although this leads to increased knee joint velocities in the stance leg, the vastly reduced knee angle lead to reduced torques [23].



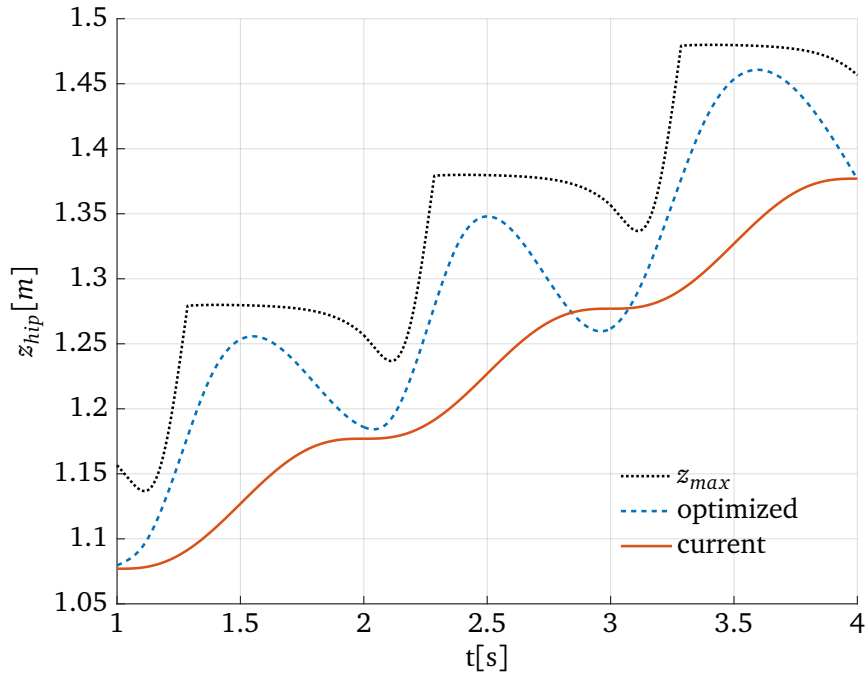


Figure 4.15: Comparison of height trajectories for upstairs movement with step size  $\Delta x = 0.4m$

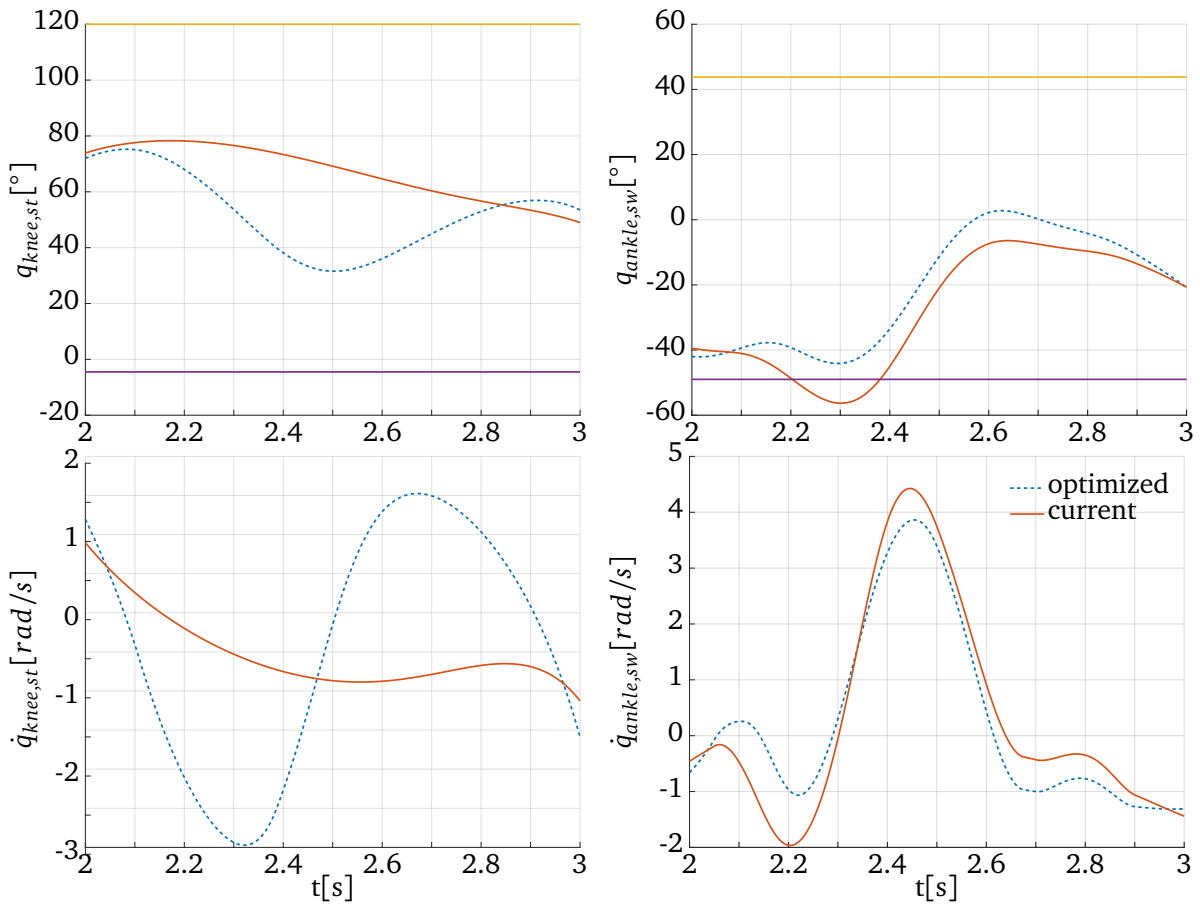
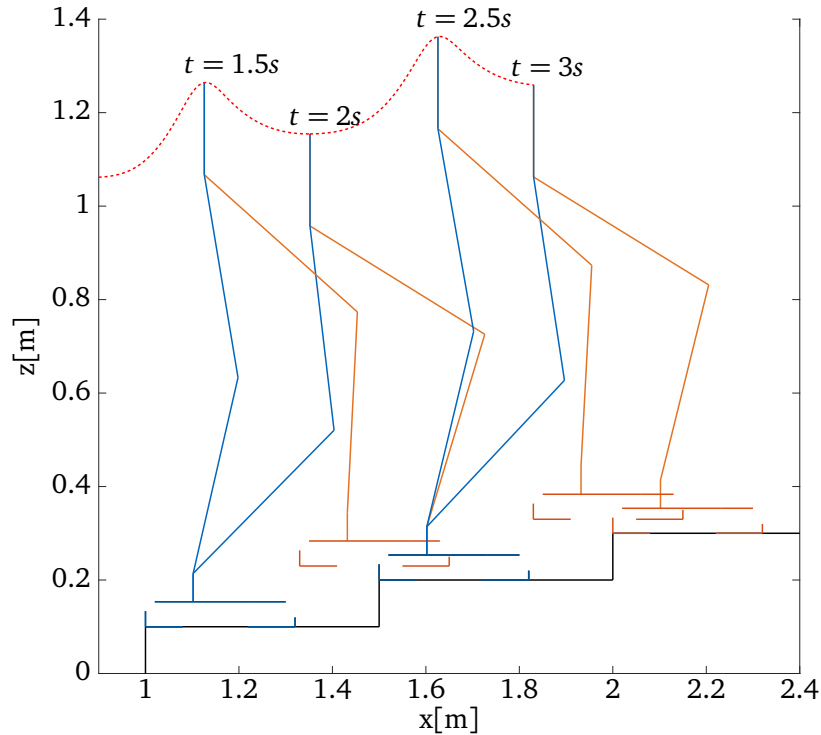


Figure 4.16: Comparison of joint angles and velocities for upstairs movement with step size  $\Delta x = 0.4m$

Looking at the joint angle of the swing foot ankle in figure 4.16 reveals a reason for the failure of the current height trajectory in upstairs walking. The joint angles and velocities correspond to the

step phase with  $2s \leq t < 3s$  from figure 4.15. In the first half of the step the ankle angle obtained for the quintic spline falls below the minimally feasible angle and the robot is therefore unable to perform the desired movement. The increased height of the optimized trajectory avoids the violation of the lower joint angle limit and additionally reduces the swing leg ankle joint velocity peaks. While kinematically possible it cannot be assessed if the strong increase and decrease of hip height necessary to follow the optimized trajectory is dynamically feasible here. This is subject to further investigation in a dynamic simulation.



**Figure 4.17:** Intermediate stepping poses for upstairs movement with optimized trajectory

Figure 4.17 shows the resulting movement of the optimized trajectory. The red curve represents the hip height trajectory in cartesian space. The poses correspond to points in time of figure 4.15. At  $t = 2s$  the robot is in mid dual-stance. The leg in blue on the lower stair is the swing leg of the upcoming step. The ankle joint of this swing leg is the critical joint in this maneuver. The ankle joint angle decreases further if the hip advances in x-direction without simultaneously increasing the hip height sufficiently. An alternative solution would be to raise the heel off the ground while maintaining contact with the foot pad. This solution is motivated by human walking. Currently heel off walking is not implemented on the humanoid robot *Lola*.

### 4.3.3 Downstairs

In the case of downstairs movement similar problems occur. Figure 4.18 compares the trajectories in the optimized and currently used generation method. The planned heights differ as much as  $0.10m$ . The optimized trajectory covers more of the allowable range of hip heights and closely approaches the upper bound given by the maximum hip height. Please note that the trajectories do not start at the same initial height in this plot. In the first step phase not illustrated both trajectories start with the same initial height. This first step is used to allow the optimized hip height trajectory to adapt to a steady state hip height. The currently used quintic spline cannot start at the same height  $z = 1.45m$  at time  $t = 1s$  because the trajectory would then violate the maximum hip height.

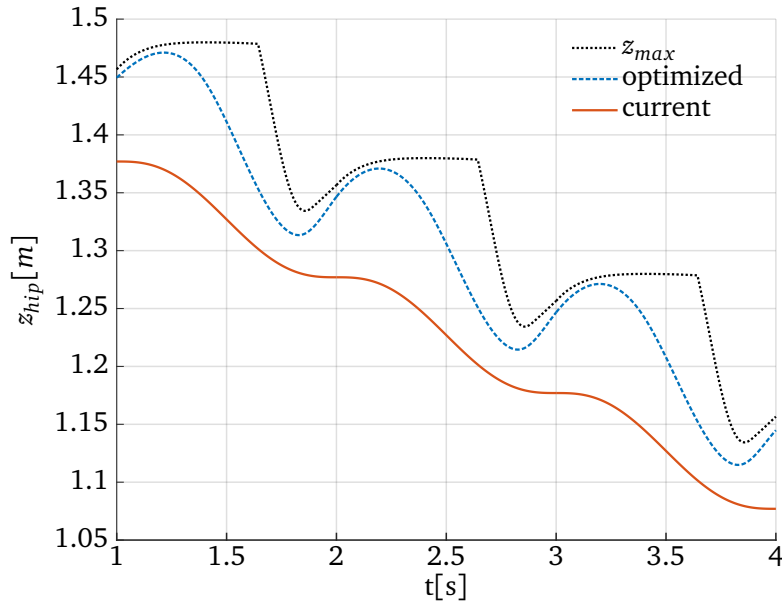


Figure 4.18: Comparison of height trajectories for downstairs movement with step size  $\Delta x = 0.4m$

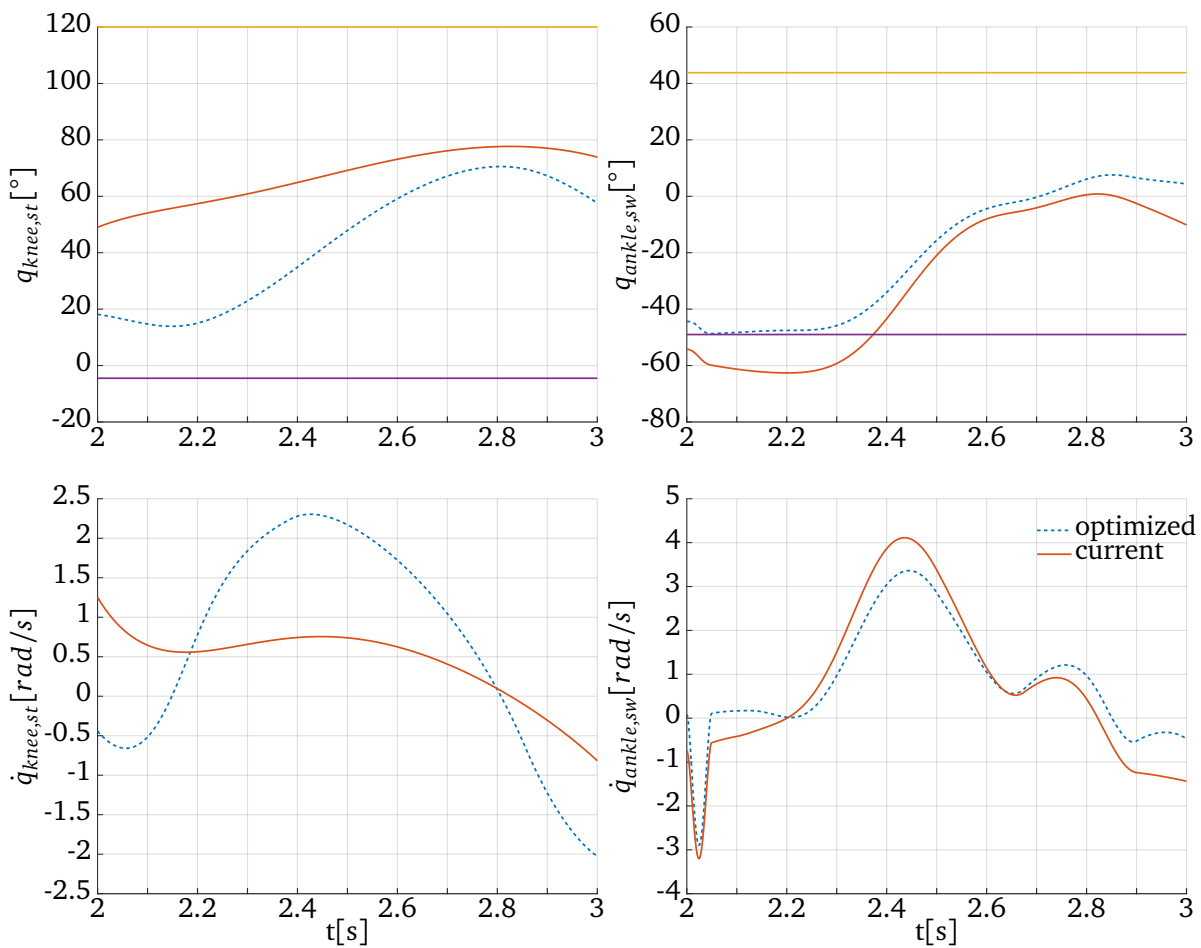
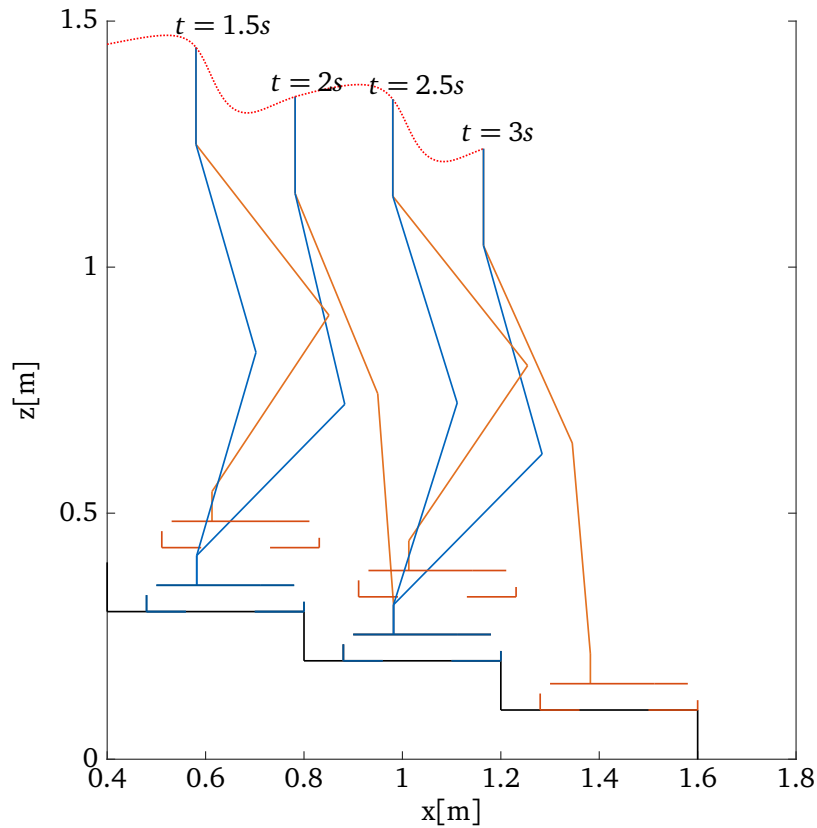


Figure 4.19: Comparison of joint angles and velocities for downstairs movement with step size  $\Delta x = 0.4m$

Comparing the joint angles and velocities for one step phase in particular in figure 4.19 yields findings similar to before in the upstairs case. The optimized trajectory leads to a greatly reduced

stance knee angle of up to  $42^\circ$  lower than for the current trajectory. In contrast to the upstairs case this deviation is already at the beginning of the step phase. The minimally reached knee joint angle is with about  $q_{knee,st} = 14^\circ$  still far enough away from the knee singularity. As before the possible advantage of lower knee angles leading to lower torque can only be mentioned but not assessed.

The threat of ankle angle limits being violated in downstairs walking is present as well. The currently used quintic spline trajectory exceeds the lower angle limit of  $q_{ankle,min} = -49^\circ$  by more than  $10^\circ$ . The optimized trajectory yields a technically feasible ankle joint trajectory. With a safety margin of as low as  $0.3^\circ$ , however, this might not be favorable. Also for downstairs motion the peaks of the ankle joint velocity can be reduced by employing the optimized trajectory rather than the currently used one.



**Figure 4.20:** Intermediate stepping poses for downstairs movement with optimized trajectory

The visualization of intermediate stepping poses of the robot in figure 4.20 gives a rationale for why the possible ankle joint limit violation occurs. Directly after the beginning of the step phase at  $t = 2s$  the lowest difference between limit and ankle angle is reached. In the pose corresponding to this time  $t = 2s$  the swing leg is represented by the blue leg on the higher step. While the hip advances forward to shift weight from the former stance leg to the new stance leg, the swing leg is lifted from the higher stair. Both movements lead to a further reduction of the ankle angle. Without being able to use a heel lift off motion this can only be counteracted by increasing the hip height. The currently employed quintic spline is monotonically decreasing for downstairs movement and therefore unable to do so.

In comparison to upstairs movement the downstairs movement is more problematic concerning the ankle joint limit. The joint limit violation is prone to occur in the swing leg during the transition of weight from old to new stance leg. In the downstairs case, however, this swing leg is on higher ground and therefore the allowable hip height is limited by the stance leg standing on lower ground. This limits the ability to increase the height and also leads to an increased ankle

joint angle from the start. It also explains why the joint limit in the ankle can only be closely avoided by the optimized trajectory in 4.19.

## 4.4 Discussion

### 4.4.1 Input Trajectories

During the search for feasible initial input trajectories to the simulation, a high dependency on the foot trajectory timings has been observed. Exemplarily this will be discussed for a change in the timings of the foot trajectory in z-direction. The example is displayed in figure 4.21 for the case of upstairs walking with  $\Delta z = 0.1m$ . The time when the peak height is reached differs by 0.1s. In the results presented prior to this section a timing of  $t_{high} = 0.5s$  was used. Both trajectories are valid in terms of avoiding collision with the stairs.

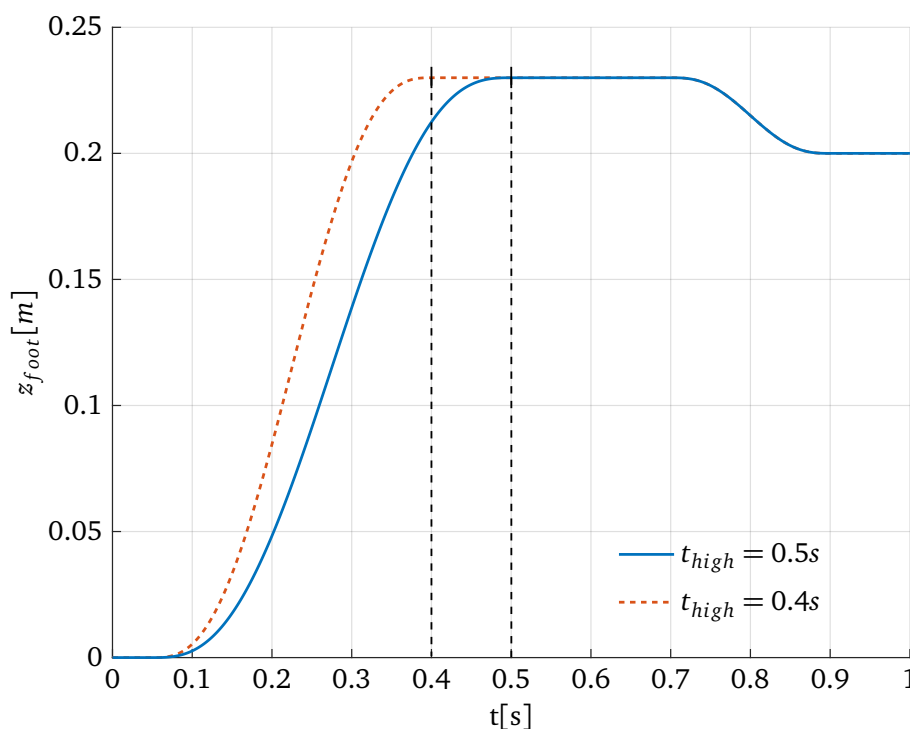


**Figure 4.21:** Changed input trajectory  $z_{foot}$  for upstairs step with  $\Delta z = 0.1m$

The resulting influence on the optimization problem of finding an appropriate height trajectory can best be seen in figures 4.22 and 4.23. The color indicates the cost at each point in time for a range of hip heights. Both joint angle violations and maximum hip height violation are considered. The joint velocity cost cannot be scanned in this manner, since its value is dependent on transient behavior. Above the maximum hip height the cost function becomes active and takes a value greater than zero. With lower heights the cost function becomes active for when joint angle limits are violated. The two peaks occurring at  $t = 1.3s$  and  $t = 2.3s$  represent the violation of the ankle joint limit. The timings correspond to the observations made in figure 4.16. The cost function scan obtained with the modified trajectory with timing  $t_{high} = 0.4s$  yields a reduced range of feasible solutions. The resulting contour plot shows a smaller corridor remaining for the hip height trajectory to pass through without violating the ankle joint limit.

Other timings of the input trajectories assumed for the simulation in the MATLAB environment have similar effects. Their validity has not been verified with trajectories from *Lola's* pattern gen-

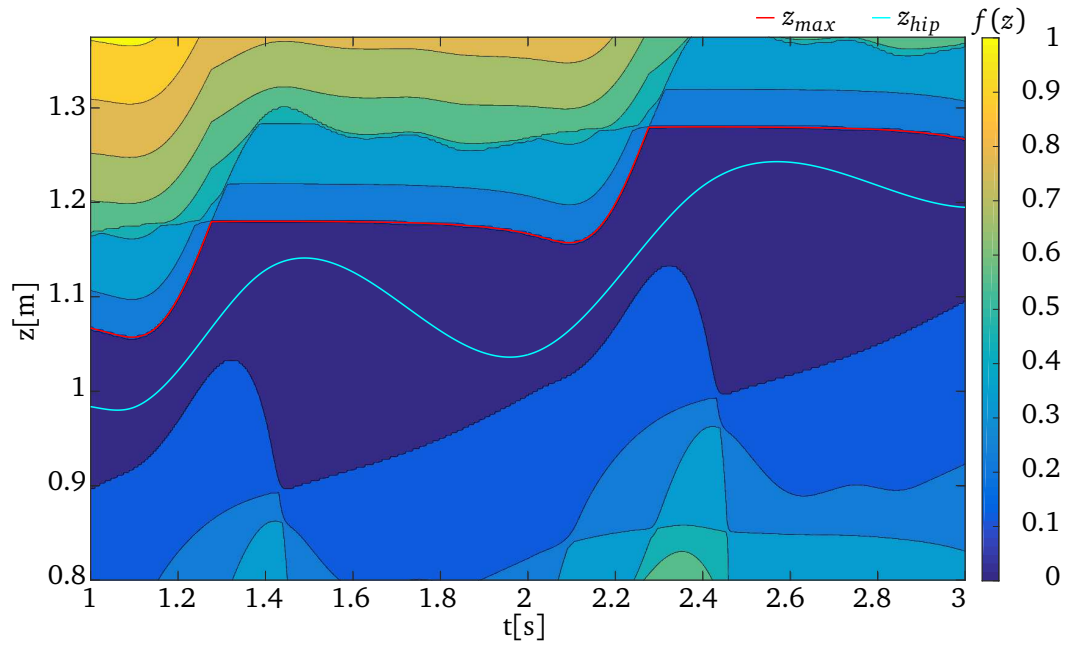


**Figure 4.22:** Cost function scan with  $t_{high} = 0.5s$  for two upstairs steps with  $\Delta z = 0.1m$

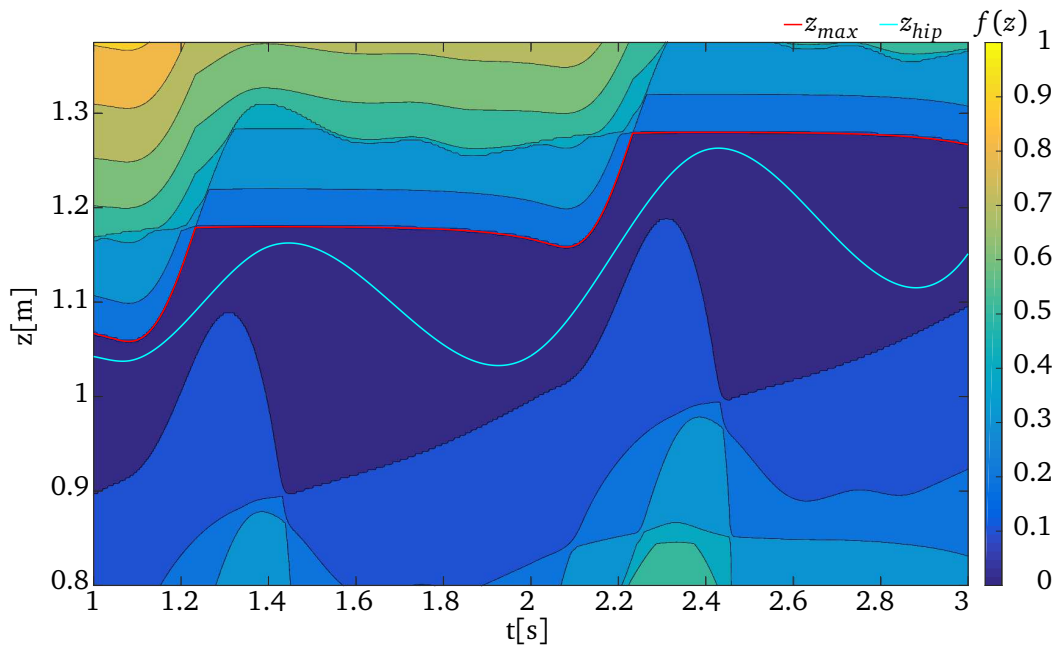


**Figure 4.23:** Cost function scan with  $t_{high} = 0.4s$  for two upstairs steps with  $\Delta z = 0.1m$

eration system. A verification of the results obtained in this simulation is therefore necessary.

#### 4.4.2 Flawed Initial Solution

It was found that the initial solution is not feasible for all scenarios. Figure 4.24 shows a scenario for when this occurs. The trajectories for three upstairs steps with a preview period of  $n = 4$  are

visualized. At step two the initial solution violates the maximum hip height for the first previewed step. The optimization still yields a feasible solution. For step three the initial solution obtained for the first previewed step is also not favorable. The resulting optimized solution does not take the usual form and lacks periodicity for the previewed steps. The results in section 4.2 show that for a lower amount of previewed steps, i.e.  $n = 2$  and  $n = 3$  the optimization is still able to find a favorable solution. For more than three previewed steps this does not always hold true. A possible explanation is the global influence of support points in the cubic splines, i.e. changing a support point influences all following spline segments. More previewed steps increase the amount of support points and an unfavorable initial solution can lead to the convergence to a different local minimum. A review of the constraints established to derive a feasible initial solution is necessary.

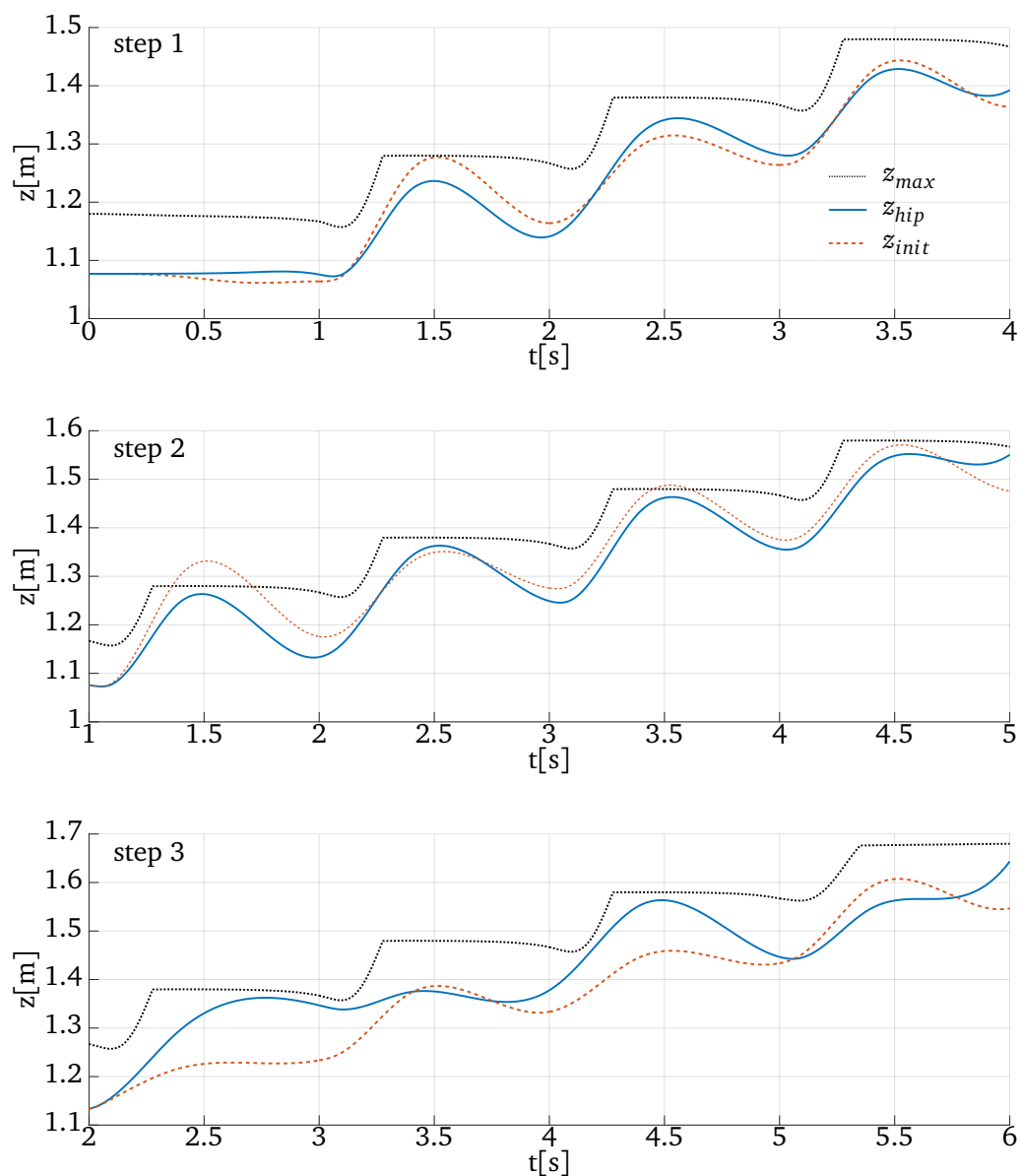


**Figure 4.24:** Poor initial solution in step three leads to bad performance of optimization result for preview period of  $n = 4$

### 4.4.3 Performance

For all investigated scenarios the new height trajectory generation method could improve the performance compared to the currently employed formulation. The knee singularity could be avoided for large step lengths in even walking. During upstairs and downstairs walking joint limits are not violated as they would be with the currently used approach. Furthermore knee angles could be reduced which could lead to a reduction in torques acting on the robot joints. Considering the shortcomings mentioned in section 4.1.3 these results and their applicability to the particular scenarios should be taken qualitatively rather than quantitatively. The general potential of the proposed hip height trajectory generation to achieve improvements particularly for uneven walking has been shown.



## Chapter 5

### Conclusion

A new approach to generate a variable hip height trajectory was proposed in this work. The principal aim was to improve the locomotion of the humanoid robot *Lola* in uneven terrain. Ongoing research in the respective field was presented and categorized for its applicability. The scope of the existing robot control framework was briefly presented to explore implications for the proposed system.

According to the given environment and motivated by different publications a new approach was developed combining some of their concepts to generate the vertical hip trajectory. In order to consider kinematic limits the concept of the maximum hip height was adopted. It was included in an optimization based approach of finding a feasible trajectory. The initial solution for this optimization problem was derived following the requirement to be kinematically feasible. To achieve this, a representation using cubic splines was chosen and constrained according to kinematic limits and the observation of characteristics. The goal of the optimization was formulated based on both the maximum hip height and a simple geometric model to assure low execution time while staying within the allowable range of solutions. Another optimization goal was to minimize joint velocities of the robot. To further improve the results the scope of the optimization was extended to following steps.

In order to assess the feasibility of the proposed method a simulation environment implemented in MATLAB was formulated. Several simplifying assumptions were necessary for this evaluation. As input to the proposed method robot trajectories for feet and hip were assumed. Multiple scenarios were simulated for walking in even and uneven environment. The new approach was able to yield kinematically feasible results in all subjected scenarios. A comparison to the currently used hip height trajectory showed lower joint velocities for the new formulation.

In the context of the simplifying assumptions made this can be seen as a step towards implementing and testing the proposed method on the actual robot. Before achieving this some open problems remain. Finding a feasible initial trajectory, especially for kinematically challenging stepping scenarios with big step lengths or heights, has proven to be difficult. This issue needs to be resolved, by either reiterating the formulation of the initial solution constraints or by assuring convergence in real-time. In order to integrate the obtained trajectory into the existing framework a transformation from hip height to Center of Mass (CoM) height has to be formulated.

After successfully incorporating the trajectory generation method in the control system of *Lola* further verification is necessary. Simulations and experiments can show if the assumptions made are applicable. The implications of considering motion in 2D rather than 3D and the dependency on the feet and horizontal CoM trajectories could possibly be adopted to. A stronger restriction applies, if the dynamic limits of the robot are exceeded by the newly proposed trajectory. The simple model did not account for dynamic effects.

Regarding the many possibilities of improvement by employing a variable CoM height a successful integration into the pattern generation system of the humanoid robot *Lola* is considered favorable even if some restrictions may apply.

## Appendix A

### Additional Plots

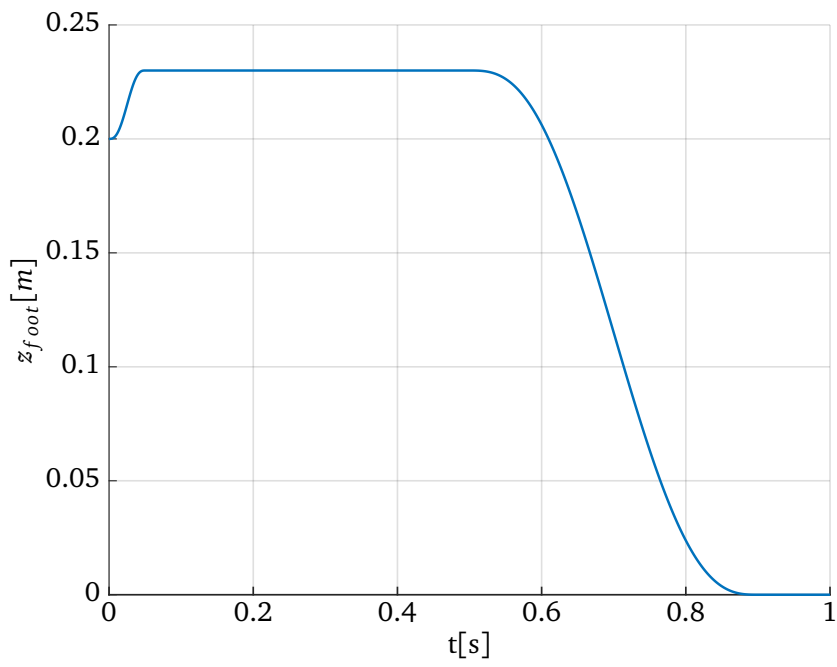


**Figure A.1:** Foot trajectory in z-direction for downstairs with  $\Delta z = -0.1$

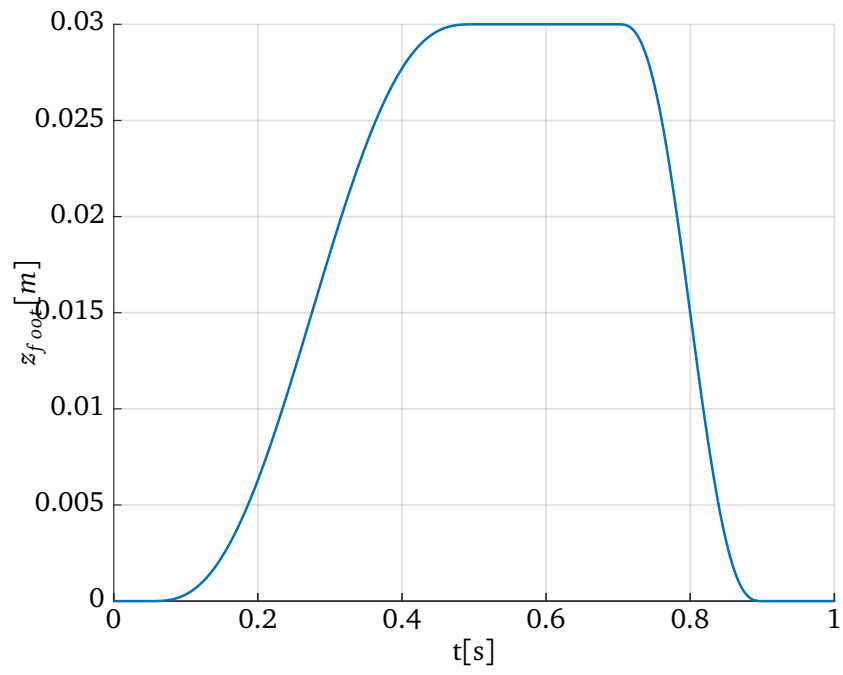


**Figure A.2:** Foot trajectories in z-direction for even walking

## Bibliography

- [1] Andriacchi, T. P., Ogle, J. A., and Galante, J. O. „Walking speed as a basis for normal and abnormal gait measurements“. In: *Journal of Biomechanics* 10.4 (1977), pp. 261–268.
- [2] Brasseur, C., Sherikov, A., Collette, C., Dimitrov, D., and Wieber, P.-B. „A robust linear MPC approach to online generation of 3D biped walking motion“. In: *IEEE-RAS International Conference on Humanoid Robots*. Ed. by IEEE. 2015, pp. 595–601.
- [3] Buschmann, T. *Simulation and control of biped walking robots: Techn. Univ., Diss.–München, 2010*. 1. Aufl. München: Verl. Dr. Hut, 2011.
- [4] Buschmann, T., Lohmeier, S., Bachmayer, M., Ulbrich, H., and Pfeiffer, F. „A collocation method for real-time walking pattern generation“. In: *IEEE-RAS International Conference on Humanoid Robots*. Ed. by IEEE. 2007, pp. 1–6.
- [5] Chenglong Fu and Ken Chen. „Gait Synthesis and Sensory Control of Stair Climbing for a Humanoid Robot“. In: *IEEE Transactions on Industrial Electronics* 55.5 (2008), pp. 2111–2120.
- [6] Chevallereau, C. and Aoustin, Y. „Self-stabilization of 3D walking via vertical oscillations of the hip“. In: *IEEE International Conference on Robotics and Automation*. Ed. by IEEE. 2015, pp. 5088–5093.
- [7] Clever, D. and Mombaur, K. „A new template model for optimization studies of human walking on different terrains“. In: *IEEE-RAS International Conference on Humanoid Robots*. Ed. by IEEE. 2014, pp. 500–505.
- [8] Engelsberger, J., Ott, C., and Albu-Schaffer, A. „Three-dimensional bipedal walking control using Divergent Component of Motion“. In: *IEEE/RSJ International Conference on Intelligent Robots and Systems*. Ed. by IEEE. 2013, pp. 2600–2607.
- [9] Herdt, A., Perrin, N., and Wieber, P.-B. „LMPC based online generation of more efficient walking motions“. In: *IEEE-RAS International Conference on Humanoid Robots*. Ed. by IEEE. 2012, pp. 390–395.
- [10] Hildebrandt, A.-C., Wahrmann, D., Wittmann, R., Rixen, D., and Buschmann, T. „Real-time pattern generation among obstacles for biped robots“. In: *IEEE/RSJ International Conference on Intelligent Robots and Systems*. Ed. by IEEE. 2015, pp. 2780–2786.
- [11] Hildebrandt, A.-C., Wittmann, R., Wahrmann, D., Ewald, A., and Buschmann, T. „Real-time 3D collision avoidance for biped robots“. In: *IEEE/RSJ International Conference on Intelligent Robots and Systems*. Ed. by IEEE. 2014, pp. 4184–4190.
- [12] Hof, A. L. „The 'extrapolated center of mass' concept suggests a simple control of balance in walking“. In: *Human movement science* 27.1 (2008), pp. 112–125.
- [13] Hong, Y.-D. and Lee, K.-B. „Dynamic simulation of modifiable bipedal walking on uneven terrain with unknown height“. In: *Journal of Electrical Engineering and Technology*. Vol. 11, no. 3. 2016, pp. 733–740.

- [14] Hong, Y.-D., Park, C.-S., and Kim, J.-H. „Stable Bipedal Walking With a Vertical Center-of-Mass Motion by an Evolutionary Optimized Central Pattern Generator“. In: *IEEE Transactions on Industrial Electronics* 61.5 (2014), pp. 2346–2355.
- [15] Hopkins, M. A., Hong, D. W., and Leonessa, A. „Humanoid locomotion on uneven terrain using the time-varying divergent component of motion“. In: *IEEE-RAS International Conference on Humanoid Robots*. Ed. by IEEE. 2014, pp. 266–272.
- [16] Kajita, S., Kanehiro, F., Kaneko, K., Fujiwara, K., Harada, K., Yokoi, K., and Hirukawa, H. „Biped walking pattern generation by using preview control of zero-moment point“. In: *IEEE International Conference on Robotics and Automation*. Ed. by IEEE. 2003, pp. 1620–1626.
- [17] Kajita, S., Matsumoto, O., and Saigo, M. „Real-time 3D walking pattern generation for a biped robot with telescopic legs“. In: *IEEE Midwest Symposium on Circuits and Systems*. Ed. by IEEE. 2000, pp. 2299–2306.
- [18] Koichi Nishiwaki, Satoshi Kagami, Nishiwaki, K., and Kagami, S. „Online design of torso height trajectories for walking patterns that takes future kinematic limits into consideration“. In: *IEEE International Conference on Robotics and Automation*. Ed. by IEEE. 2011, pp. 2029–2034.
- [19] Kolter, J. Z. and Ng, A. Y. „Task-space trajectories via cubic spline optimization“. In: *IEEE International Conference on Robotics and Automation*. Ed. by IEEE. 2009, pp. 1675–1682.
- [20] Kudruss, M., Naveau, M., Stasse, O., Mansard, N., Kirches, C., Soueres, P., and Mombaur, K. „Optimal control for whole-body motion generation using center-of-mass dynamics for pre-defined multi-contact configurations“. In: *IEEE-RAS International Conference on Humanoid Robots*. Ed. by IEEE. 2015, pp. 684–689.
- [21] Lack, J. „Integrating the effects of angular momentum and changing center of mass height in bipedal locomotion planning“. In: *IEEE-RAS International Conference on Humanoid Robots*. Ed. by IEEE. 2015, pp. 651–656.
- [22] Li, Z., Tsagarikis, N. G., Caldwell, D. G., and Vanderborght, B. „Trajectory generation of straightened knee walking for humanoid robot iCub“. In: *International Conference on Control, Automation, Robotics & Vision*. Ed. by IEEE. 2010, pp. 2355–2360.
- [23] Li, Z., Vanderborght, B., Tsagarakis, N. G., and Caldwell, D. G. „Fast bipedal walk using large strides by modulating hip posture and toe-heel motion“. In: *IEEE International Conference on Robotics and Biomimetics*. Ed. by IEEE. 2010, pp. 13–18.
- [24] Miura, K., Morisawa, M., Kanehiro, F., Kajita, S., Kaneko, K., and Yokoi, K. „Human-like walking with toe supporting for humanoids“. In: *IEEE/RSJ International Conference on Intelligent Robots and Systems*. Ed. by IEEE. 2011, pp. 4428–4435.
- [25] Morisawa, M., Kajita, S., Kaneko, K., Harada, K., Kanehiro, F., Fujiwara, K., and Hirukawa, H. „Pattern Generation of Biped Walking Constrained on Parametric Surface“. In: *IEEE International Conference on Robotics and Automation*. Ed. by IEEE. 2005, pp. 2405–2410.
- [26] Moro, F. L., Tsagarakis, N. G., and Caldwell, D. G. „Efficient human-like walking for the compliant huMANoid COMAN based on linematic Motion Primitives (kMPs)“. In: *IEEE International Conference on Robotics and Automation*. Ed. by IEEE. 2012, pp. 2007–2014.
- [27] Nishiwaki, K., Chestnutt, J., and Kagami, S. „Autonomous navigation of a humanoid robot over unknown rough terrain using a laser range sensor“. In: *The International Journal of Robotics Research* 31.11 (2012), pp. 1251–1262.
- [28] Nishiwaki, K. and Kagami, S. „Online Walking Control System for Humanoids with Short Cycle Pattern Generation“. In: *The International Journal of Robotics Research* 28.6 (2009), pp. 729–742.

- [29] Nishiwaki, K., Chestnutt, J., and Kagami, S. „Planning and Control of a Humanoid Robot for Navigation on Uneven Multi-scale Terrain“. In: *Experimental Robotics*. Ed. by Khatib, O., Kumar, V., and Sukhatme, G. Vol. 79. Springer Tracts in Advanced Robotics. Berlin, Heidelberg: Springer Berlin Heidelberg, 2014, pp. 401–415.
- [30] Nishiwaki, K. and Kagami, S. „Simultaneous planning of CoM and ZMP based on the preview control method for online walking control“. In: *IEEE-RAS International Conference on Humanoid Robots*. Ed. by IEEE. 2011, pp. 745–751.
- [31] Nishiwaki, K. and Kagami, S. „Trajectory design and control of edge-landing walking of a humanoid for higher adaptability to rough terrain“. In: *IEEE/RSJ International Conference on Intelligent Robots and Systems*. Ed. by IEEE. 2012, pp. 3432–3439.
- [32] Ogura, Y., Shimomura, K., Kondo, A., Morishima, A., Okubo, T., Momoki, S., Hun-ok Lim, and Takanishi, A. „Human-like walking with knee stretched, heel-contact and toe-off motion by a humanoid robot“. In: *IEEE/RSJ International Conference on Intelligent Robots and Systems*. Ed. by IEEE. 2006, pp. 3976–3981.
- [33] Park, C.-S., Ha, T., Kim, J., and Choi, C.-H. „Trajectory generation and control for a biped robot walking upstairs“. In: *International Journal of Control, Automation and Systems* 8.2 (2010), pp. 339–351.
- [34] Pratt, J., Carff, J., Drakunov, S., and Goswami, A. „Capture Point: A Step toward Humanoid Push Recovery“. In: *IEEE-RAS International Conference on Humanoid Robots*. Ed. by IEEE. 2006, pp. 200–207.
- [35] Qiang Huang, Yokoi, K., Kajita, S., Kaneko, K., Arai, H., Koyachi, N., and Tanie, K. „Planning walking patterns for a biped robot“. In: *IEEE Transactions on Robotics and Automation* 17.3 (2001), pp. 280–289.
- [36] Sardain, P. and Bessonnet, G. „Forces Acting on a Biped Robot. Center of Pressure—Zero Moment Point“. In: *IEEE Transactions on Systems, Man, and Cybernetics - Part A: Systems and Humans* 34.5 (2004), pp. 630–637.
- [37] Shafii, N., Lau, N., and Reis, L. P. „Learning a fast walk based on ZMP control and hip height movement“. In: *IEEE International Conference on Autonomous Robot Systems and Competitions*. Ed. by IEEE. 2014, pp. 181–186.
- [38] Shin, H.-K. and Kim, B. K. „Energy-Efficient Gait Planning and Control for Biped Robots Utilizing Vertical Body Motion and Allowable ZMP Region“. In: *IEEE Transactions on Industrial Electronics* 62.4 (2015), pp. 2277–2286.
- [39] Siyuan Feng, Xinjilefu, X., Weiwei Huang, and Atkeson, C. G. „3D walking based on online optimization“. In: *IEEE-RAS International Conference on Humanoid Robots*. Ed. by IEEE. 2013, pp. 21–27.
- [40] Staufenberg, N.-S. „Evaluierung alternativer Fußtrajektorien für einen humanoiden Laufroboter“. Semester Thesis. München: Technische Universität München, 2016.
- [41] Takenaka, T., Matsumoto, T., and Yoshiike, T. „Real time motion generation and control for biped robot -1st Report: Walking gait pattern generation-“. In: *IEEE/RSJ International Conference on Intelligent Robots and Systems*. Ed. by IEEE. 2009, pp. 1084–1091.
- [42] Takenaka, T., Matsumoto, T., Yoshiike, T., and Shirokura, S. „Real time motion generation and control for biped robot -2nd report: Running gait pattern generation-“. In: *IEEE/RSJ International Conference on Intelligent Robots and Systems*. Ed. by IEEE. 2009, pp. 1092–1099.
- [43] Tobias Blume. „Development and Kinematic Optimization of a Novel Collision-Free Swing Foot Trajectory for a Humanoid Robot“. Diploma Thesis. München: Technische Universität München, 25.06.2015.

- [44] van Heerden, K. „Planning COM trajectory with variable height and foot position with reactive stepping for humanoid robots“. In: *IEEE International Conference on Robotics and Automation*. Ed. by IEEE. 2015, pp. 6275–6280.
- [45] Vukobratovic, M. and Juricic, D. „Contribution to the Synthesis of Biped Gait“. In: *IEEE Transactions on Biomedical Engineering* BME-16.1 (1969), pp. 1–6.
- [46] Wahrmann, D., Hildebrandt, A.-C., Wittmann, R., Sygulla, F., Rixen, D., and Buschmann, T. „Fast object approximation for real-time 3D obstacle avoidance with biped robots“. In: *IEEE International Conference on Advanced Intelligent Mechatronics*. Ed. by IEEE. 2016, pp. 38–45.
- [47] Yi, S.-J., Hong, D., and Lee, D. D. „Heel and toe lifting walk controller for traversing uneven terrain“. In: *IEEE-RAS International Conference on Humanoid Robots*. Ed. by IEEE. 2015, pp. 325–330.
- [48] Zhao, Y. and Sentis, L. „A three dimensional foot placement planner for locomotion in very rough terrains“. In: *IEEE-RAS International Conference on Humanoid Robots*. Ed. by IEEE. 2012, pp. 726–733.

## Disclaimer

I hereby declare that this thesis is entirely the result of my own work except where otherwise indicated. I have only used the resources given in the list of references.

Garching, 30. October 2016

---

(Signature)